Excitonic mechanism for superconductivity in a quasi-one-dimensional system

J. E. Hirsch
Department of Physics, University of California, San Diego, La Jolla, California 92093

D. J. Scalapino
Department of Physics, University of California, Santa Barbara, California 93106
(Received 24 August 1984; revised manuscript received 20 March 1985)

The properties of a one-dimensional electron-exciton model are studied using weak- and strong-coupling perturbation theory, along with Monte Carlo simulations in the intermediate-coupling regime. We focus on the charge-density wave (CDW) and singlet-pairing susceptibilities, and determine their behavior as functions of the parameters in the Hamiltonian. We also discuss the properties of an array of weakly coupled chains. Our conclusions are that for a single chain it is possible, although difficult, to have pairing correlations dominate over CDW correlations. For an array of weakly coupled chains, however, it is highly unlikely that one would obtain a transition to a superconducting state.

I. INTRODUCTION

Since Bardeen, Cooper, and Schrieffer[1] (BCS) explained the mechanism responsible for superconductivity through the electron-phonon interaction, there has been an ongoing search for materials that exhibit superconductivity through an alternative mechanism. The driving force behind this search is that another mechanism (particularly if electronic in origin) might possibly be able to circumvent the limitation on the attainable values of the critical temperatures imposed by the electron-phonon mechanism. No such material has been found to date.

In 1964, Little proposed a detailed model for a superconductor based on an electronic excitation (exciton) mechanism rather than a phonon mechanism.[2] The basic idea of the model is that conduction electrons residing on one type of molecules would induce electronic transitions on neighboring polarizable molecules, which would provide an effective attractive interaction between the conduction electrons. With electronic energies being much larger than phonon energies, Little argued that such a system would possibly exhibit high-temperature (room-temperature or higher) superconductivity.

Although the excitonic mechanism proposed by Little could occur in any number of dimensions, Little and later workers[3] argued that the most favorable situation would occur in quasi-one-dimensional systems, where it would be possible to densely pack highly polarizable molecules around a conducting spine. Little's proposal was the initial catalyst for work on quasi-one-dimensional organic compounds. Although a wealth of interesting physics as well as practical applications have emerged from these studies,[4] the goal of synthesizing a high-temperature organic superconductor has remained elusive to date.

On the theoretical side, there have been a variety of studies ranging from mean-field BCS-like theories to renormalization group and bosonization calculations. The large fluctuations in one-dimensional systems make a pairing mean-field theory and random-phase-approximation (RPA) screening of the interaction suspect. In addition, there is always the question of vertex corrections. In one-dimensional systems there is the additional complication of dealing with other competing instabilities. Renormalization-group (RG) methods can deal with these problems, and for weak-coupling instantaneous interactions they have been used to obtain ground-state phase diagrams.[5,6] However, retardation is an essential feature of an exciton-mediated interaction, and further approximations and assumptions are required to reduce a retarded interaction to a form which can be treated within the RG framework.[7] In addition, it is difficult to assess the range of validity of these RG calculations, and whether they are valid for realistic parameters in the relevant temperature region.

In this paper, we study a one-dimensional (1D) electron-exciton model using a variety of techniques. We discuss weak-coupling perturbation theory, strong-coupling perturbation theory, and Monte Carlo simulations in the intermediate-coupling regime. We also make use of renormalization-group results in the weak- and strong-coupling regimes. The Monte Carlo simulations are particularly useful in tying together the results obtained from the various asymptotic regimes, and indicating which theoretical results should be taken seriously and which should not. They also are useful in indicating that no exotic new phenomena occur at intermediate-coupling regimes.

We focus on the behavior of various susceptibilities which signal the tendency toward different types of order in the chain. Our main interest lies in the competition between charge-density-wave (CDW) and singlet-pairing (SP) susceptibilities and their dependence on various parameters in the Hamiltonian, particularly retardation effects, and band filling. The great advantage of Monte Carlo simulations is that we can obtain information on these susceptibilities for finite chains essentially without any approximation. By studying chains of different sizes, we can extract conclusions about the properties of the system in the thermodynamic limit.

Among workers in the field, opinion has been divided regarding whether a quasi-one-dimensional system of the type considered here is a good candidate for a high-

temperature superconductor.[3] We believe that ours is the first comprehensive study of this system over the whole parameter range, and that we can draw some quite definitive conclusions on this question. As discussed in Sec. V, our main conclusion is that it is very unlikely that a model such as the one discussed in this paper will ever be found to display superconductivity at any temperature.

The outline of this paper is as follows: in Sec. II we define the model and discuss the quantities of interest to study. In Sec. III we discuss various theoretical results: the noninteracting chain, low-order weak-coupling perturbation theory, and strong-coupling perturbation theory. In Sec. IV we discuss the Monte Carlo algorithm used and present results of simulations for various cases. Finally, we summarize our conclusions in Sec. V.

Part of the results presented in this paper were reported briefly elsewhere.[8]

II. ELECTRON-EXCITON MODEL

The model we consider consists of weakly coupled chains of the type originally suggested by Little.[2] Each chain has a one-dimensional conducting backbone surrounded by polarizable side groups. The Hamiltonian for a chain has the form

$$H=\sum_{\sigma,l}[-t(d^{\dagger}_{zz\sigma l+1}d_{zz\sigma l}+\text{H.c.})-\mu n_{zz\sigma l}] + \sum_{l}[-\bar{t}(d^{\dagger}_{xzl}p_{zl}+\text{H.c.})+\epsilon_{xz}n_{xzl}+\epsilon_{pz}n_{pz}] + \sum_{l}(Un_{zz\uparrow l}n_{zz\downarrow l}+\bar{U}n_{zzl}n_{xzl}) . \quad (2.1)$$

A possible realization of this Hamiltonian is shown schematically in Fig. 1. It consists of a linear stack of equally spaced transition-metal complexes whose d_{zz} orbitals overlap through a one-electron transfer integral t. The "polarizable side groups" arise from the hybridization of the d_{zx} orbitals of each metal atom with the π orbitals of its surrounding ligand complex represented here by a p_z orbital. The d_{xz}-p_z overlap matrix element $\bar{t}$ sets the scale of the excitation energy. Here we will assume that the site energies ϵ_{xz} and ϵ_{pz} are such that the bonding hybridized state lies well below the Fermi energy μ of the d_{zz} band, while its antibonding partner lies well above μ. As in the Hubbard model, we keep the on-site d-orbital repulsive Coulomb interactions U and $\bar{U}$. Later we will also discuss the effects of near-neighbor Coulomb interactions.

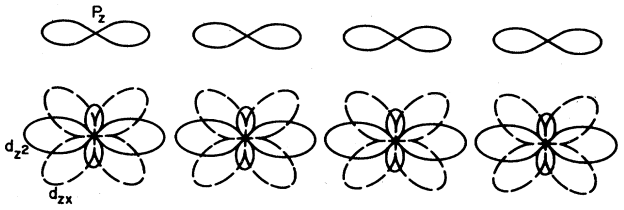

FIG. 1. Schematic of one possible realization of Little's model of an electron-exciton chain.

Although both U and $\bar{U}$ are repulsive, it is important to understand the different roles they play. The direct Coulomb interaction U among the d_{zz} electrons favors a spin density wave state. The d_{zz}-d_{xz} Coulomb interaction $\bar{U}$ gives rise to an exciton mediated interaction between the d_{zz} electrons which favors pairing or charge density wave correlations. Through $\bar{U}$, a d_{zz} electron can virtually excite a d_{xz}-ligand electron from its lower energy state to its higher energy state leading to a local polarization. If the energy transfer is less than the splitting of the d_{xz}-ligand states, then the polarization will produce an attractive potential for a second d_{zz} electron. This mechanism gives rise to an attractive exciton mediated interaction. A central question is whether it will (i) generate a static clumping of electrons along the spine forming a charge density wave, or (ii) induce a pairing state in which there is a power law decay of the pair-pair correlations.

In general the π band of the ligands surrounding the metal mix with both the d_{xz} and the d_{yz} orbitals of the metal. In addition, these states will have a spin quantum number. Here we absorb these factors into the coupling $\bar{U}$ and, for simplicity in our simulation, treat the excitonic electrons as spinless fermions. In addition, screening due to orbitals not explicitly included can alter the relative sizes of U and $\bar{U}$. The rational for neglecting near-neighbor Coulomb couplings, which we will do for much of this study, is simply an example of this. Nevertheless, in drawing conclusions regarding the physical properties of this model it is useful to remember that on an isolated atom U and $\bar{U}$ are related by Clebsch-Gordan coefficients, and thus it would be unphysical to keep $\bar{U}$ while neglecting U.

The nature of the correlations of an individual chain can be conveniently characterized in terms of the behavior of the zero-frequency momentum-dependent charge-density, spin-density, singlet- and triplet-pairing susceptibilities:

$$\chi_{\text{CDW}}(q)=\frac{1}{N}\sum_{l,j,\sigma,\sigma'}e^{iq(l-j)}\int_0^{\beta}d\tau[\langle n_{l\sigma}(\tau)n_{j\sigma'}(0)\rangle-\langle n_{l\sigma}(\tau)\rangle\langle n_{j\sigma'}(0)\rangle] , \quad (2.2a)$$

$$\chi_{\text{SDW}}(q)=\frac{1}{N}\sum_{l,j}e^{iq(l-j)}\int_0^{\beta}d\tau\langle[n_{l\uparrow}(\tau)-n_{l\downarrow}(\tau)][n_{j\uparrow}(0)-n_{j\downarrow}(0)]\rangle , \quad (2.2b)$$

$$\chi_{\text{SP}}(q)=\frac{1}{N}\sum_{l,j}e^{iq(l-j)}\int_0^{\beta}d\tau\langle d^{\dagger}_{l\downarrow}(\tau)d^{\dagger}_{l\uparrow}(\tau)d_{j\uparrow}(0)d_{j\downarrow}(0)\rangle , \quad (2.2c)$$

$$\chi_{\text{TP}}(q)=\frac{1}{N}\sum_{l,j}e^{iq(l-j)}\int_0^{\beta}d\tau\langle d^{\dagger}_{l\uparrow}(\tau)d^{\dagger}_{l+1\uparrow}(\tau)d_{j+1\uparrow}(0)d_{j\uparrow}(0)\rangle . \quad (2.2d)$$

Here all the operators refer to the d_{zz} band and we have dropped the zz subscript.

At any finite temperature, these susceptibilities are, of course, finite. However, as the temperature decreases toward zero, divergent peaks can occur at characteristic values of the momentum. Typically, charge- and spin-density waves with $q=2p_F$ and pairing correlations at $q=0$ are studied. In addition, the compressibility of the electrons [$\chi_{\rm CDW}(0)$] can be of interest. For a commensurate filling, such as $\rho=1.0$, the ground state can have long-range CDW order. However, quantum fluctuations destroy long-range order when phase fluctuations can occur, leaving only power-law correlations for SDW, SP, TP, and incommensurate CDW ground states. This power-law behavior also manifests itself in the low-temperature structure of the susceptibilities. For example, the space-imaginary time, singlet-pairing correlation function in the Luttinger model has the form

$$\left[\frac{1}{x^2+(v_F\tau)^2}\right]^{1/2\theta} . \tag{2.3}$$

Here θ depends upon the interaction parameters. At a finite temperature T, the correlations decay exponentially when $x \gtrsim v_F/T$. Thus the singlet-pairing $q=0$ susceptibility varies at low temperatures as

$$\chi_{\rm SP}(q=0)=\int_0^\beta d\tau \int_0^{v_F\beta}\left[\frac{1}{x^2+(v_F\tau)^2}\right]^{1/2\theta} \sim \left[\frac{1}{T}\right]^{2-1/\theta} . \tag{2.4}$$

In general, the susceptibilities at low temperatures vary as $T^{-\mu}$ and one says, for example, that a chain is in the SP state if $\mu_{\rm sp}$ is larger than all the other μ's.

Coupling between the chains can occur through a direct Coulomb interaction $V_\perp$ as well as by a one-electron transfer $t_\perp$. The Coulomb interaction favors CDW formation while the one-electron transfer in second order can lead to a stabilization of all types of order. Besides leading to the formation of a three-dimensional (3D) charge-density-wave state, it can give rise to a superexchange coupling the SDW's or a Josephson pair transfer coupling SP or TP correlations. Treating the coupling between chains within a mean-field approximation[9,10] and the electron transfer as local and instantaneous, the transition temperatures for 3D ordering are given by

$$\begin{aligned} 1&=ZV_\perp\chi_{\rm CDW}(2p_F) , \\ 1&=Z\frac{t_\perp^2}{\Delta}\chi_{\rm SDW}(2p_F) , \\ 1&=Z\frac{t_\perp^2}{\Delta}\chi_{\rm SP}(0) , \\ 1&=Z\frac{t_\perp^2}{\Delta}\chi_{\rm TP}(0) . \end{aligned} \tag{2.5}$$

Here Z is the number of near-neighbor chains, and Δ is an effective energy gap associated with transferring an electron from one chain to another. We have assumed that $V_\perp$ determines the CDW order rather than the $t_\perp$ suppression of the 1D fluctuations. Thus, the phase of a quasi-one-dimensional system depends upon both the single chain susceptibility and the interchain coupling.

Here we focus on the susceptibilities of a single chain and their dependence on the parameters of H, the band filling ρ, and the temperature T. Following a discussion of analytic results available for various limiting cases we turn to results for the susceptibilities (2.2) obtained from numerical simulations of the electron-exciton model described by Eq. (2.1).

III. THEORETICAL BACKGROUND

In this section we begin with a calculation of the charge-density and singlet-pairing susceptibilities for a noninteracting finite chain. This will allow us to understand how one can extract the behavior of the infinite chain from results for finite chains. Following this, the frequency and momentum dependence of the exciton mediated interaction and its consequences in lowest-order perturbation theory for the charge-density and pairing responses will be investigated. Then we will conclude with discussions of the weak-coupling and strong-coupling limits which provide a framework for the numerical simulations discussed in Sec. IV.

A. Noninteracting chain problem

For a noninteracting d_{zz} chain,

$$\chi_{\rm CDW}(q)=2\sum_p \frac{f(\epsilon_{p+q})-f(\epsilon_p)}{\epsilon_p-\epsilon_{p+q}} , \tag{3.1}$$

and

$$\chi_{\rm SP}(q)=\sum_p \frac{1-f(\epsilon_{p+q})-f(\epsilon_p)}{\epsilon_p+\epsilon_{p+q}} , \tag{3.2}$$

with $\epsilon_p=-2t\cos p-\mu$. Figure 2 shows $\chi_{\rm CDW}(q)$ and $\chi_{\rm SP}(q)$ at three different temperatures for a 16-site chain with a quarter-filled band $\rho=\langle n_{zz}\rangle=0.5$. As the temperature is lowered, characteristic peaks at $q=2p_F$ and 0 begin to grow in the CDW and SP susceptibilities, respectively. Figure 3 shows a plot of these peak heights $\chi_{\rm CDW}(2p_F)$ and $\chi_{\rm SP}(0)$ versus β for chains of length $N=8$, 12, and 16. From this one sees that a finite chain length N begins to cause deviations when the thermal coherence length $v_F\beta$ exceeds $N/2$. Thus a useful approach for extracting data for different temperatures is to scale N with β. Figure 4 shows results for $\chi_{\rm CDW}(2p_F)$ and $\chi_{\rm SP}(0)$ obtained using $\beta=N/4$ for $N=8$, 12, 16, 20, and 24 site lattices. The solid curves are the infinite lattice extrapolation. This clearly shows the $\ln\beta$ divergence of these susceptibilities with a slope equal to $N(0)=(\pi v_F)^{-1}$. We will make use of similar scaling procedures to analyze the Monte Carlo data obtained from interacting finite chains.

B. Exciton interaction

In order to understand the behavior of the susceptibilities for an interacting system, it is useful to begin by looking at the structure of the interaction. In the absence of $\overline{U}$, Eq. (2.1) describes a Hubbard model with an instan-

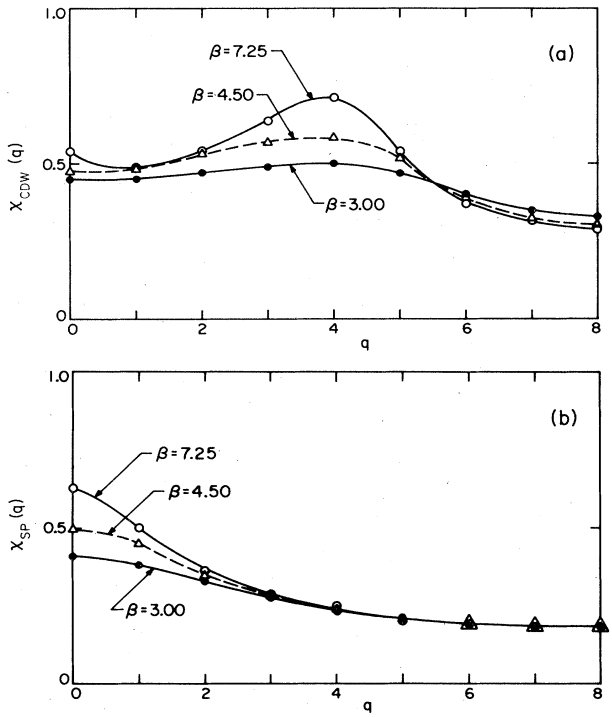

FIG. 2. (a) $\chi_{CDW}(q)$ and (b) $\chi_{SP}(q)$ versus q for a noninteracting 16-site ring with $\rho=0.5$ and $\beta=3$, 4.5, and 7.25.

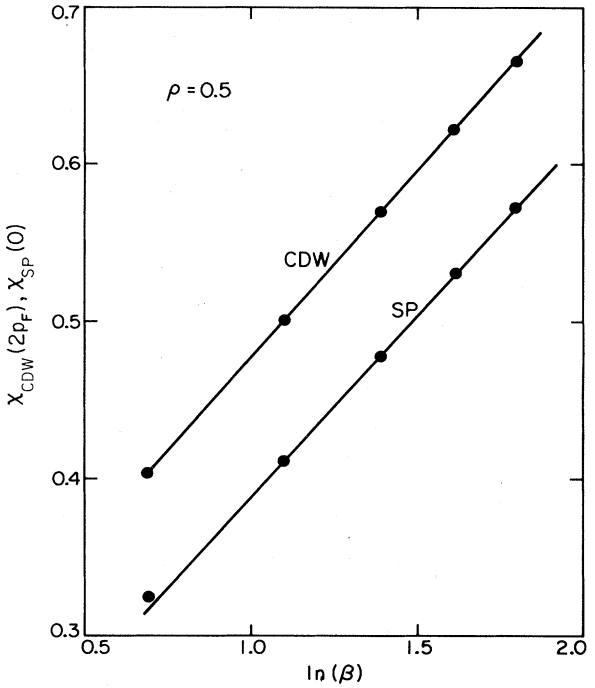

FIG. 4. Scaling results for $\chi_{CDW}(2p_F)$ and $\chi_{SP}(0)$ for the noninteracting case. Here we have taken $\beta=N/4$. The solid lines are the results for an infinite chain.

taneous local repulsive interaction U. This type of interaction favors the SDW response. When $\bar{U}\neq 0$, it couples the d_{zz} band to the local d_{zz}-p_z excitons which gives rise to an effective d_{zz}-d_{zz} interaction mediated by the excitons. The lowest-order perturbation-theory diagram for the exciton mediated interaction is shown in Fig. 5. Here a d_{zz} electron excites the d_{zz}-p_z bonding state to the antibonding state via the Coulomb interaction $\bar{U}n_{zz}n_{zx}$. The polarized d_{zx}-p_z state then scatters a d_{zz} electron, giving rise to an effective interaction of the form

$$V_{\text{eff}}=\frac{2\bar{U}^2\bar{t}^2/(E_+-E_-)}{\omega^2-(E_+-E_-)^2+i\delta}\ . \tag{3.3}$$

Here E_+-E_- is the energy difference between the antibonding and bonding d_{zx}-p_z states. Neglecting the effects of the Coulomb interaction, this energy difference is $[(2\bar{t})^2+(\epsilon_{pz}-\epsilon_{dzx})^2]^{1/2}$, so that if $\epsilon_{pz}-\epsilon_{dzx}=0$, one has

$$V_{\text{eff}}=\frac{\bar{U}^2\bar{t}}{\omega^2-4\bar{t}^2+i\delta}\ . \tag{3.4}$$

If the exciton splitting $2\bar{t}$ is large compared to the energy

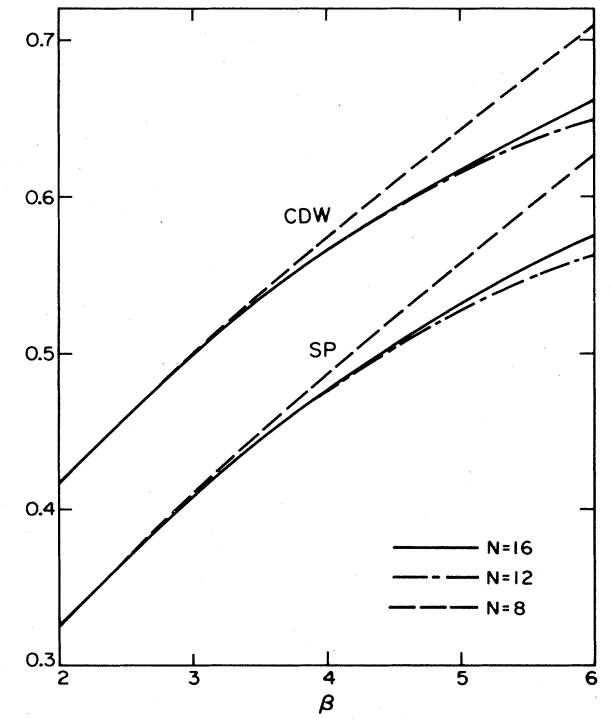

FIG. 3. Plot of peak heights $\chi_{CDW}(2p_F)$ and $\chi_{SP}(0)$ for noninteracting rings of 8, 12, and 16 sites versus β.

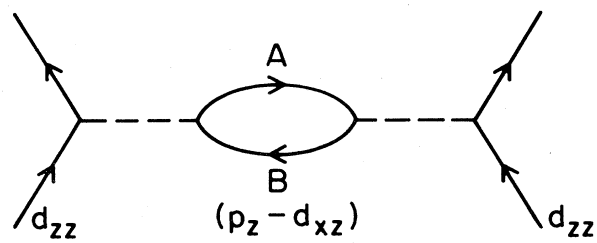

FIG. 5. Lowest-order $\bar{U}^2$ contribution to the exciton mediated interaction between d_{zz} electrons. The dashed lines represent $\bar{U}$ and the lines labeled A and B represent the antibonding and bonding p_z-d_{xz} states, respectively.

transfer ω, then V_{eff} can be approximated by an effective on-site attractive interaction $-\bar{U}^2/4\bar{t}$.

The usual RPA approximation for the CDW response sums the bubble graphs while for SP the ladder graphs are summed. In 1D however, all of the susceptibilities given by Eq. (2.2) have low-temperature logarithmic divergences so that RG techniques have been used to treat the various channels on an equal footing. Here, in order to obtain a qualitative feeling for the effect of retardation we begin by calculating the first-order bubble and ladder contributions to CDW and SP shown in Figs. 6(a) and 6(b), respectively. In these graphs, the effective exciton mediated interaction of Fig. 5 is represented by the wavy line. Note that for $\chi_{\text{CDW}}(2p_F)$, Fig. 6(a), the interaction carries momentum $q=2p_F$ and $\omega=0$, because we are interested in the zero frequency response. Thus, the contribution of Fig. 6(a) to $\chi_{\text{CDW}}(2p_F)$ for a half-filled band ($2p_F=\pi$) is

$$\frac{4}{\beta^2}\sum_{n,n'}\sum_{p,p'}\frac{1}{\omega_n^2+\epsilon_p^2}\frac{\bar{U}^2}{4\bar{t}}\frac{1}{\omega_{n'}^2+\epsilon_{p'}^2} . \tag{3.5}$$

Here $\omega_n=\pi(2n+1)kT$ and $\omega_{n'}$ are the usual Matsubara fermion frequencies and $\epsilon_p=-2t\cos(p)$ is the band energy measured relative to the d_{zz} chemical potential μ which is zero for a half-filled band. Note that independent of the ratio $\bar{t}/t$, the effective interaction appearing in Eq. (3.5) is the nonretarded limit of Eq. (3.4). This is not the case for the singlet-pairing contribution shown in Fig. 6(b). This term contributes to $\chi_{\text{SP}}(0)$,

$$\frac{1}{\beta^2}\sum_{n,n'}\sum_{p,p'}\frac{1}{\omega_n^2+\epsilon_p^2}\frac{1}{\omega_{n'}^2+\epsilon_{p'}^2}\frac{\bar{U}^2\bar{t}}{(\omega_n-\omega_{n'})^2+4\bar{t}^2} . \tag{3.6}$$

Here we clearly see the retarded aspect of the effective interaction. In the same way, the first-order vertex correction to the polarization is reduced by retardation. Since its contribution differs in sign from that of Fig. 6(a), this effect of retardation actually enhances the $\chi_{\text{CDW}}(2p_F)$ response.

Carrying out the momentum sums in Eq. (3.6) for a half-filled band, one obtains

$$\frac{1}{\beta^2}\sum_{n,n'}\frac{1}{|\omega_n|(\omega_n^2+4t^2)^{1/2}}\frac{1}{|\omega_{n'}|(\omega_{n'}^2+4t^2)^{1/2}}\times\frac{\bar{U}^2\bar{t}^2}{(\omega_n-\omega_{n'})^2+4\bar{t}^2} . \tag{3.7}$$

When $\bar{t}\gg t$, the interaction is essentially instantaneous and has strength $\bar{U}^2/4\bar{t}$. In this case, the sums are cut off when ω_n and $\omega_{n'}$ are of order $2t$, and one obtains

$$\left[\frac{1}{2\pi t}\right]^2\frac{\bar{U}^2}{4\bar{t}}\ln^2(4t/\pi kT) . \tag{3.8}$$

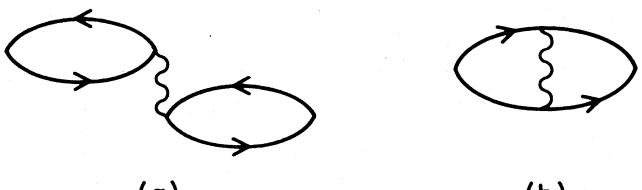

FIG. 6. First-order bubble and ladder contributions to (a) CDW and (b) SP susceptibilities.

However, when $\bar{t}\lesssim t$ the retarded nature of the interaction reduces its effective strength by $[(\omega_n-\omega_{n'})^2/4\bar{t}^2+1]^{-1}$. Figure 7 shows

$$\left\langle\frac{1}{(\omega_n-\omega_{n'})^2/4\bar{t}^2+1}\right\rangle = \frac{\sum_{n,n'}F(n,n')[(\omega_n-\omega_{n'})^2/4\bar{t}^2+1]^{-1}}{\sum_{n,n'}F(n,n')} , \tag{3.9}$$

with

$$F(n,n')=[|\omega_n|(\omega_n^2+4t^2)^{1/2}|\omega_{n'}|(\omega_{n'}^2+4t^2)^{1/2}]^{-1}$$

for different $\bar{t}/t$ values. As $\bar{t}/t$ is reduced, retardation, decreases the ratio of the effective interaction of pairing relative to the instantaneous part which enters the CDW bubble diagrams.[11] A rough estimate of this effect can be obtained by replacing the exciton interaction, Eq. (3.4), by the separable form

$$V_{\text{eff}}=\begin{cases}\dfrac{-\bar{U}^2}{4\bar{t}} & \text{for } |\omega_n|<2\bar{t} \text{ and } |\omega_m|<2\bar{t},\\ 0 \text{ otherwise.}\end{cases} \tag{3.10}$$

In this case, when $2\bar{t}$ is less than or of order $4t$, V_{eff} provides the cutoffs in Eq. (3.6), and $4t$ in Eq. (3.8) is replaced by $2\bar{t}$. This leads to the dashed curve shown in Fig. 7.

It is also useful to consider the effect of the spatial structure of the effective interaction. The on-site structure of the Coulomb coupling in Eq. (2.1) leads to a momentum independent interaction, Eq. (3.4). However, as noted, we will also consider the effect of a near-neighbor coupling,

$$\sum_l \bar{V}n_{zzl}(n_{zx\,l+1}+n_{zx\,l-1}) . \tag{3.11}$$

In terms of the effective interaction shown in Fig. 5, this modifies Eq. (3.3) by a factor $[1+(2\bar{V}/\bar{U})\cos(q)]^2$, where q is the momentum carried by the effective interaction. Here we will consider the case of a one-quarter-filled band with $2p_F=\pi/2$ and assume $\bar{t}\gg t$. Then since $\cos\pi/2$ vanishes, the interaction entering the CDW diagram, Fig.

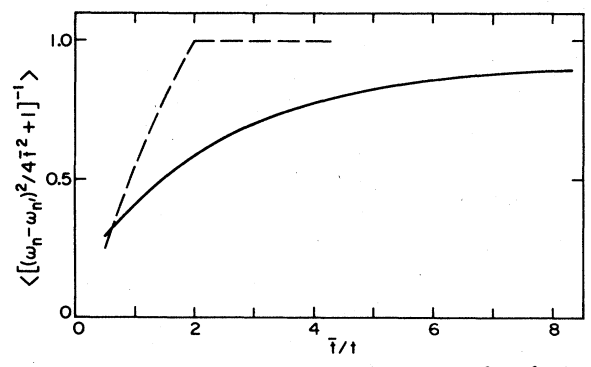

FIG. 7. The solid curve shows $\langle[(\omega_n-\omega_{n'})^2/4\bar{t}^2+1]^{-1}\rangle$ versus $\bar{t}/t$ for $\beta=4$. The dashed curve is the two-cutoff ("g-ology") approximation.

6(a), remains the same as before. However, the pairing contribution of Fig. 6(b) is

$$\sum_{p,p'} \frac{\tanh(\beta\epsilon_p/2)}{2\epsilon_p} \frac{\tanh(\beta\epsilon_{p'}/2)}{2\epsilon_{p'}} \frac{\bar{U}^2}{4\bar{t}} \left[1+\frac{2\bar{V}}{\bar{U}}\cos(p-p')\right]^2 . \tag{3.12}$$

Here we have carried out the frequency sums. Taking the ratio of Eq. (3.12) to its value for $\bar{V}=0$ gives an average enhancement factor $\langle[1+(2\bar{V}/\bar{U})\cos(p-p')]^2\rangle$ of the pairing interaction to the $q=2p_F$ part of the interaction which enters the $\chi_{\rm CDW}(2p_F)$ contribution of Fig. 6(a). Thus, as is well known, a spatially extended interaction enhances the momentum averaged interaction which enters the pairing response relative to the large $2p_F$ momentum part of the effective interaction which enters the CDW response. It is also possible to have a momentum dependence in the effective interaction due to banding effects of the d_{xz}-p_z states. However, we find that due to cancellations this gives rise to only small changes from the q independent case.

These are, of course, first-order perturbation-theory results. However, they clearly show that the space-time (q,ω) structure of the exciton mediated interaction is important. In a one-dimensional system, charge-density-wave formation is favored over pairing by a retarded $(\bar{t}/t \ll 1)$ and local (on-site) interaction.

C. Weak-coupling results

If for the moment we assume that $\bar{t}$ is sufficiently large that the exciton interaction can be treated as nonretarded and relatively weak, the results of the weak-coupling RG are of interest. Here we have an effective contact interaction,

$$U_{\rm eff}=-\frac{\bar{U}^2}{4\bar{t}}+U , \tag{3.13}$$

so that the coupling constants characterizing the large momentum $(2p_F)g_1$ and the small momentum g_2 transfer parts of the interaction are equal,

$$g_1=g_2=U_{\rm eff} . \tag{3.14}$$

For $U_{\rm eff}<0$, an attractive Hubbard model, the perturbation-theoretic RG equations scale the spin degrees of freedom to a strong-coupling limit with a gap Δ and the charge degrees of freedom to weak coupling such that for $kT<\Delta$,

$$\mu_{\rm CDW}=2-\theta ,$$

and (3.15)

$$\mu_{\rm SP}=2-1/\theta .$$

Here θ is given by

$$\theta=\left[\frac{1-U_{\rm eff}/2\pi v_F}{1+U_{\rm eff}/2\pi v_F}\right]^{1/2} . \tag{3.16}$$

For $U_{\rm eff}<0$, $\theta>1$, and $\chi_{\rm SP}(0)$ is predicted to diverge more rapidly than $\chi_{\rm CDW}(2p_F)$.

Larkin and Sak[12] found that for general ρ, Δ is given by

$$\Delta=8(2/\pi)^{1/2}\sin^2(\pi\rho/2)(\,|\,U_{\rm eff}\,|\,/\pi v_F)^{1/2} \times\exp(\pi v_F/|\,U_{\rm eff}\,|) . \tag{3.17}$$

When $kT\gg\Delta$, the spin degrees of freedom contribute to the indices reducing the rate of divergence,

$$\mu_{\rm CDW}=2-2\theta ,$$
$$\mu_{\rm SP}=2-\theta^{-1}-\theta . \tag{3.18}$$

For the half-filled case, $\rho=1$, the negative Hubbard model is predicted to have $\mu_{\rm SP}=\mu_{\rm CDW}=1$.

Now, as discussed previously, the exciton interaction is retarded. In order to treat this within the RG framework, a two-cutoff approach has been used.[7,13] This is based upon the separable approximation for the exciton-mediated interaction given by Eq. (3.10). Here the effects of retardation are put into the cutoff $2\bar{t}$ for the excitonic parts $-\bar{U}^2/4\bar{t}$ of the (g_1,g_2) couplings. When $2\bar{t}<4t$ and the degrees of freedom associated with the high-energy region of the phase space are eliminated reducing the cutoff from $4t$ to $2\bar{t}$, the g_1 part of the excitonic coupling is renormalized to

$$\bar{g}_1^e=\frac{-\bar{U}^2}{4\bar{t}}\frac{1}{1-(\bar{U}^2/4\bar{t})\ln(4t/2\bar{t})} . \tag{3.19}$$

This renormalization arises from polarization insertions which are important for momentum transfers of $q=2p_F$. Physically, what has happened is that decreasing the cutoff removed states which previously provided significant screening for momentum transfer near $2p_F$. Thus, if one removes these states, the effective g_1 coupling must be increased. The small momentum transfer interaction g_2 is not changed. From the g-ology diagram shown in Fig. 8 for a non-half-filled band, we see that the effect of retardation is to move the system from the SP regime toward the CDW regime. The crossover point is set by

$$\bar{g}_1^e=2g_2 , \tag{3.20}$$

which is drawn in the $\bar{t}$-$\bar{U}$ plane in Fig. 9.

D. Strong-coupling results

In an early paper, Pincus, Chaikin, and Coll[14] showed how to construct a strong-coupling approximation for the attractive Hubbard model. For $U_{\rm eff}<0$ and $|\,U_{\rm eff}\,|\gg t$, they showed that to second order in the transfer integral t, the attractive Hubbard model could be mapped onto an isotropic Heisenberg antiferromagnet. This approach was further developed by a number of workers.[15–17] For the exciton model, Eq. (2.1), it is also possible to construct a strong-coupling solution.[18,19] The site Hamiltonian is

$$h=\epsilon_{xz}n_{xz}+\epsilon_{pz}n_{pz}-\mu n_{zz}+\bar{U}n_{xz}n_{zz} + Un_{zz\uparrow}n_{zz\downarrow}-\bar{t}(p_z^\dagger d_{xz}+d_{xz}^\dagger p_z) . \tag{3.21}$$

In the manifold of states in which $n_{xz}+n_{pz}=1$, the eigenstates of h have energies given by

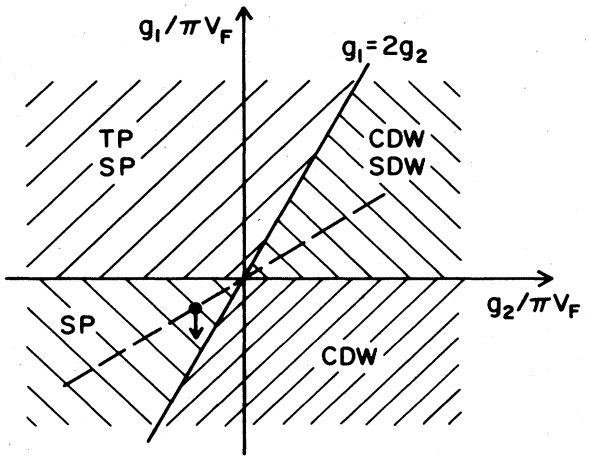

FIG. 8. Phase diagram (g_1,g_2) showing the RG predictions for a non-half-filled band. Here we have indicated the phases with the highest degree of divergence. The exciton model has $g_1=g_2$ and if $\bar{t}<2t$, g_1 is renormalized to more negative values as the cutoff is changed from $4t$ to $2\bar{t}$ moving the system toward the CDW phase as indicated by the arrow.

$$E_{\pm}(n_{zz\uparrow},n_{zz\downarrow})=\frac{\epsilon_{pz}+\epsilon_{xz}+\bar{U}n_{zz}}{2} \pm\left[\left[\frac{\epsilon_{pz}-\epsilon_{xz}-\bar{U}n_{zz}}{2}\right]^2+\bar{t}^2\right]^{1/2} +Un_{zz\uparrow}n_{zz\downarrow}-\mu n_{zz}\ , \tag{3.22}$$

with $n_{zz}=n_{zz\uparrow}+n_{zz\downarrow}$. In order for the occupancy $\rho=\langle n_{zz}\rangle$ to be different from 0 or 1, μ must be fixed so that

$$2\mu=U+\bar{U}+\left[\left[\frac{\epsilon_{pz}-\epsilon_{xz}}{2}\right]^2+\bar{t}^2\right]^{1/2} -\left[\left[\frac{\epsilon_{pz}-\epsilon_{xz}-2\bar{U}}{2}\right]^2+\bar{t}^2\right]^{1/2}\ . \tag{3.23}$$

Then the ground state of a single site is twofold degenerate with $E_-(0,0)=E_-(1,1)$ and the filling ρ determines the relative number of empty $n_{zz\uparrow}=n_{zz\downarrow}=0$ to paired

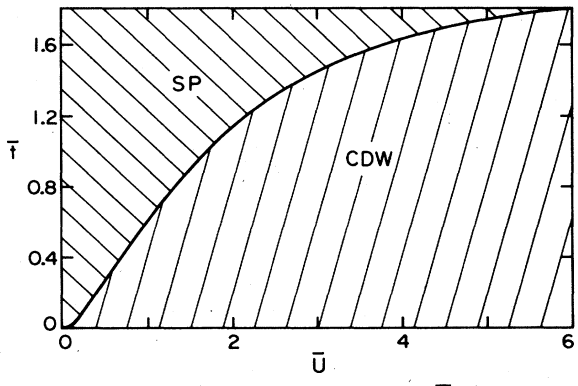

FIG. 9. Two-cutoff RG phase diagram $(\bar{t},\bar{U})$ for a non-half-filled band.

$n_{zz\uparrow}=n_{zz\downarrow}=1$ sites. The resulting ground state of a chain of N sites has energy $E_0=NE_-(0,0)$ and is highly degenerate corresponding to the number of ways $\binom{N}{N\rho/2}$ of placing $N\rho/2$ pairs on N sites. This degeneracy is lifted in second order by the hopping interaction

$$H_t=-t\sum_l (d^{\dagger}_{zz\sigma l+1}d_{zz\sigma l}+\text{H.c.})\ . \tag{3.24}$$

Let $H_0=\sum_l h(l)$ be the sum of the site Hamiltonians, then the matrix which is to be diagonalized over the degenerate manifold is

$$H_t\frac{1}{E_0-H_0}H_t\ . \tag{3.25}$$

A convenient way to express this operator is to use an effective spin representation. Here one introduces spin-$\frac{1}{2}$ operators on each site and identifies $S^z_l=\frac{1}{2}$ with a paired site $(n_{zz\uparrow l}=n_{zz\downarrow l}=1)$ and $S^z_l=-\frac{1}{2}$ with an empty site $(n_{zz\uparrow l}=n_{zz\downarrow l}=0)$. Then the process of a pair transfer from site l to site $l+1$ generated by Eq. (3.25) can be represented by

$$\sum_l \frac{J_x}{2}(S^+_{l+1}S^-_l+S^+_lS^-_{l+1})\ . \tag{3.26}$$

Here J_x involves the virtual admixing of site states with only one electron in the zz orbital. These states have energies $E_{\pm}(1,0)$ given by Eq. (3.23) and are separated by gaps $\Delta_{\pm}$ from the degenerate empty or paired-site ground states,

$$\Delta_{\pm}=E_{\pm}(n_{zz\uparrow}=1,n_{zz\downarrow}=0)-E_-(0,0)\ . \tag{3.27}$$

As discussed in the Appendix, the case where $\epsilon_{pz}-\epsilon_{xz}=\bar{U}$ is particularly symmetric and one has $\mu=\bar{U}/2$,

$$\Delta_-=[(\bar{U}/2)^2+\bar{t}^2]^{1/2}-\bar{t}-U/2\ , \tag{3.28}$$

and $\Delta_+=\Delta_-+2\bar{t}$. The lowest excited state gap Δ_- is plotted in Fig. 10 versus $\bar{U}/\bar{t}$ for various values of $\epsilon_{pz}-\epsilon_{xz}$ and $U=0$, while Fig. 11 shows Δ_- versus $\bar{U}/\bar{t}$ for $\epsilon_{pz}-\epsilon_{xz}=\bar{U}$ and $U=\bar{U}/4$.

In order to have a strong-coupling expansion, we require that the energy to break a pair into two singly occupied sites $2\Delta_-$ exceeds the hopping strength t. In our usual units where $t=1$, this implies for the symmetric case Eq. (3.28) that

$$\frac{\bar{U}^2}{1+U}-(1+U)>4\bar{t}\ . \tag{3.29}$$

The strong-coupling region in the $(\bar{t},\bar{U})$ plane is shown in Fig. 12 for $U=0$ and $U=\bar{U}/4$.

In addition to the pair transfer term, the operator in Eq. (3.25) contains an effective near-neighbor coupling,

$$\sum_l J_zS^z_lS^z_{l+1}\ . \tag{3.30}$$

Here $J_z>0$ and $J_z/2$ is the increase in energy of two neighboring pair sites which arises because of the blockage of virtual single-particle hopping processes which lower the energy of an isolated pair. Thus, the original

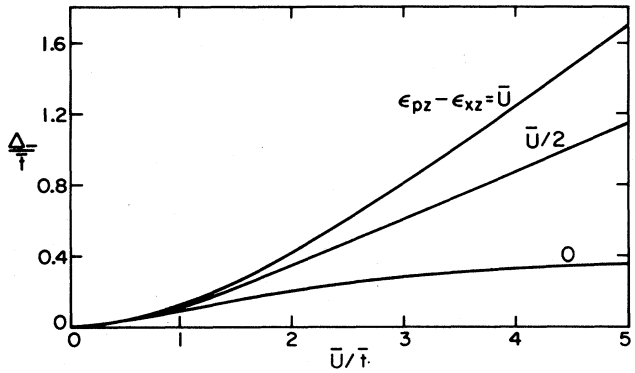

FIG. 10. The lowest excited state Δ_- versus $\bar{U}/\bar{t}$ for $\epsilon_{pz}-\epsilon_{xz}=\bar{U}$, $\bar{U}/2$, and 0. Here the on-site Coulomb interaction $U=0$.

problem associated with diagonalizing the second-order interaction Eq. (3.25) over the degenerate manifold of empty and pair-site states can be replaced by an effective XXZ antiferromagnetic model. Charge-density-wave correlations correspond to $\langle S^z_{l+i}S^z_i\rangle$ correlations and singlet-pairing correlations to $\langle S^+_{l+i}S^-_i\rangle$ correlations. The band filling ρ is given by

$$\rho=\frac{2}{N}\sum_l\langle S^z_l+\tfrac{1}{2}\rangle\ . \tag{3.31}$$

Calculation of the dependence of the coupling constants J_x and J_z on the parameters of the exciton model are given in the Appendix. In Fig. 13, the solid curves show how the ratio J_z/J_x depends upon $\bar{U}/\bar{t}$ for $U=0$ and various values of $\epsilon^{pz}-\epsilon_{xz}$. The dashed curve in Fig. 13 shows J_z/J_x versus $\bar{U}/\bar{t}$ for $\epsilon_{pz}-\epsilon_{xz}=\bar{U}$ and $U=\bar{U}/4$. From this, one sees that as $\bar{U}/\bar{t}$ increases, opening the gap so that a strong-coupling approach is suitable, the ratio J_z/J_x becomes large, and the electron-exciton system maps onto a highly anisotropic Heisenberg antiferromagnetic model.

For a half-filled band $\sum_l\langle S^z_l\rangle$ vanishes and since $J_z/J_x>1$ the spin system will be an Ising-like antiferromagnetic state. This means that the exciton system will have long range CDW order in the ground state for $\rho=1$ and for all $\bar{t}<\infty$. A similar behavior was found for a model with local electron-phonon interactions.[20] As ρ decreases (increases), the spin system will exhibit power-law

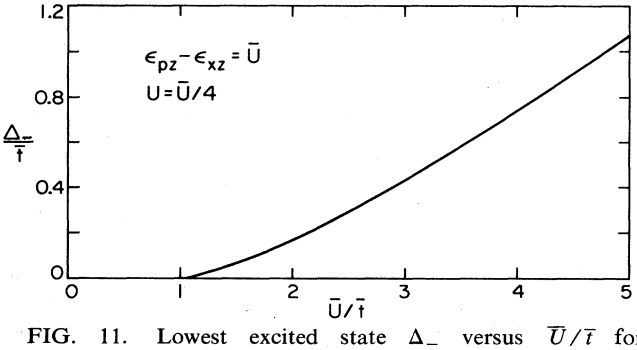

FIG. 11. Lowest excited state Δ_- versus $\bar{U}/\bar{t}$ for $\epsilon_{pz}-\epsilon_{xz}=\bar{U}$ and $U=\bar{U}/4$. Note that $\Delta_-<0$ for $\bar{U}/\bar{t}<\frac{16}{15}$.

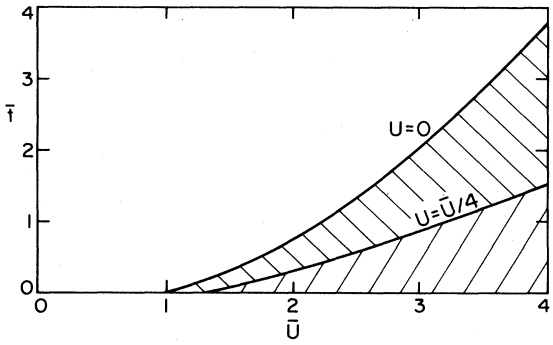

FIG. 12. The strong-coupling regime lays to the right of the curves. The value of U is shown on the curves.

structure in the longitudinal $\chi_{zz}(q\sim 2p_F)$ and transverse susceptibilities $\chi_{+-}(q\sim 0)$ for a range of J_z/J_x values. Haldane[21] has shown how Bethe ansatz results can be used to determine the correlation exponents of the XXZ system for arbitrary values of ρ. From his analysis, we obtain for $\rho=0.5$ and $\rho=0.75$ the $\mu_{\rm CDW}$ and $\mu_{\rm SP}$ results shown in Fig. 14. For $\rho=0.75$ the system exhibits a change from SP domination to CDW domination when $J_z/J_x=2.7$. For $1<J_z/J_x<2.7$, the $\chi_{\rm SP}(0)$ susceptibility diverges more rapidly than the $\chi_{\rm CDW}(2p_F)$ susceptibility, while for $2.7<J_z/J_x$ the opposite is true. As ρ is decreased further, the critical value of J_z/J_x at which this change occurs goes toward infinity. Below $\rho\cong 0.6$ (above $\rho\cong 1.4$), the $\chi_{\rm SP}(0)$ susceptibility diverges more rapidly than $\chi_{\rm CDW}(2p_F)$ for all J_z/J_x values. However, as J_z/J_x becomes increasingly large, the difference in $\mu_{\rm SP}-\mu_{\rm CDW}$ increases to a minimum value. For example, for $\rho=0.5$, $\mu_{\rm SP}\to 1.125$ and $\mu_{\rm CDW}\to 0.86$ when $J_z/J_x\to-\infty$. Thus, although as we have seen, one needs $\bar{U}/\bar{t}>2$ in order to have a sufficient gap, one wants to keep $\bar{U}/\bar{t}$ as small as possible in order to keep J_z/J_x from becoming overly large.

IV. MONTE CARLO SIMULATION

We have studied the model described by Eq. (2.1) using a Monte Carlo algorithm appropriate to a grand-canonical

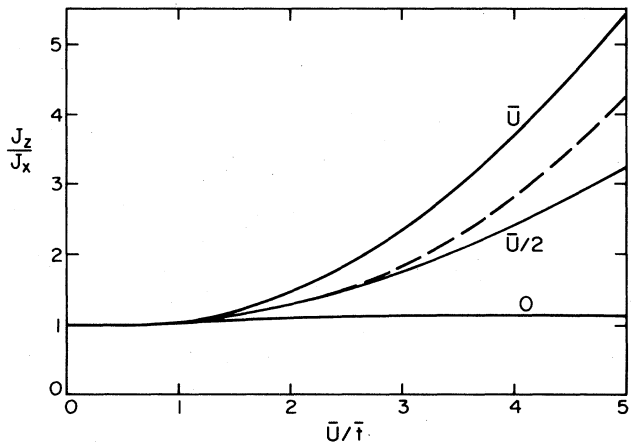

FIG. 13. The solid curves show the ratio of the effective exchange couplings J_z/J_x versus $\bar{U}/\bar{t}$ for $U=0$ and $\epsilon_{pz}-\epsilon_{xz}=\bar{U}$, $\bar{U}/2$, and 0. The dashed curve shows J_z/J_x versus $\bar{U}/\bar{t}$ with $U=\bar{U}/4$ and $\epsilon_{pz}-\epsilon_{xz}=\bar{U}$.

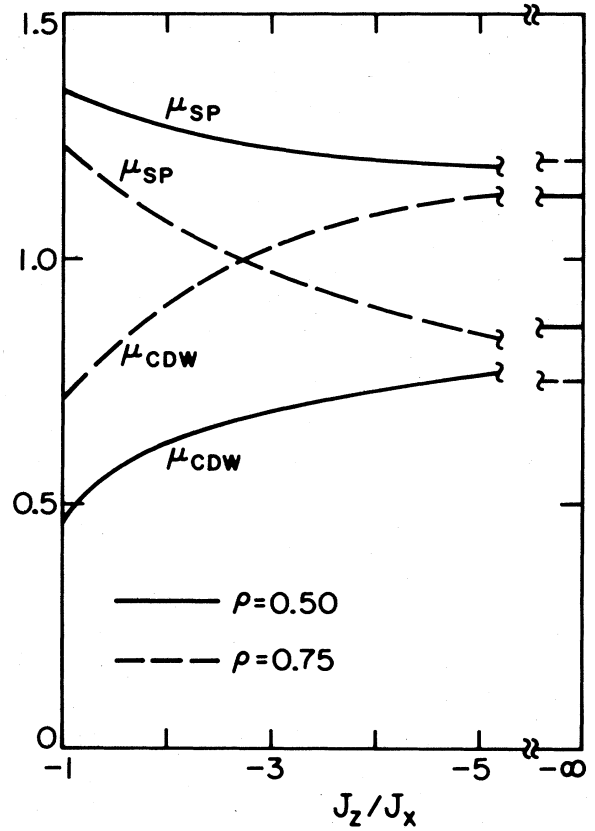

FIG. 14. μ_{CDW} and μ_{SP} versus J_z/J_x for $\rho=0.5$ (solid curve) and $\rho=0.75$ (dashed curve), from Ref. 21.

ensemble.[22] The interaction between fermions is eliminated by introducing auxiliary Ising variables,[23] the fermions are integrated out, and the fermion determinant is computed by an exact updating procedure.[22] The method has also recently been used to study two-dimensional fermion models.[24,25] For the present model, it is possible to use another algorithm, in the canonical ensemble, that does not integrate out the fermions.[26] We have also performed simulations using this latter method, which is faster and allowed us to study larger lattices. However, it is awkward to study pairing correlation functions using the canonical method, so that we mainly studied CDW correlations with it. For definiteness, we will discuss here only the result obtained with the grand-canonical algorithm. The results of the simulations with the canonical formulation were useful as a check on the grand-canonical algorithm, and also to show that nothing changed qualitatively in the CDW correlations in going to larger lattices.

We write the partition function of the system as:

$$Z=\mathrm{Tr}e^{-\beta H}=\mathrm{Tr}\left[\prod_{i=1}^{L}e^{-\Delta\tau H}\right]$$

$$\cong\mathrm{Tr}\left[\prod_{i=1}^{L}e^{-\Delta\tau H_0^{zz}}e^{-\Delta\tau H_0^{xz}}e^{-\Delta\tau V^{zz}}e^{-\Delta\tau V^{xz}}\right], \quad (4.1)$$

with

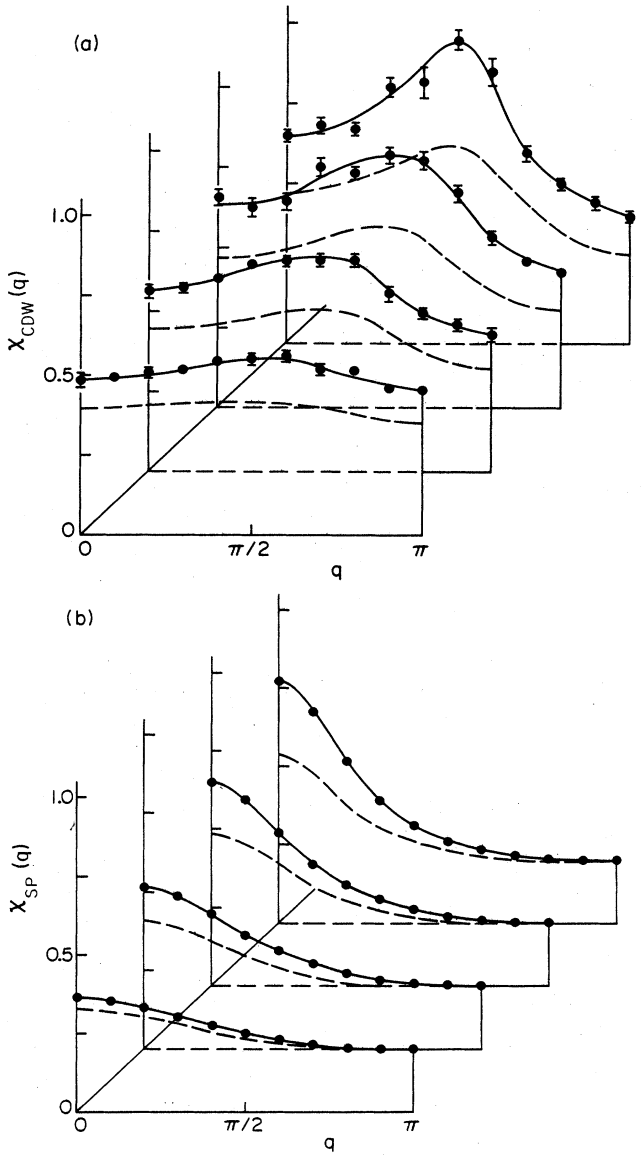

FIG. 15. (a) $\chi_{CDW}(q)$ and (b) $\chi_{SP}(q)$ versus q for a 20-site lattice at different temperatures ($\beta=2$, 3, 4, 5) with $\bar{U}=2.83$, $\bar{t}=2$, $\epsilon=\bar{U}/2$, and $U=0$. The dashed curves show the susceptibilities for the noninteracting system.

$$H_0^{zz}=\sum_{\sigma,l}-t(d_{zz\sigma l+1}^{\dagger}d_{zz\sigma l}+\mathrm{H.c.})$$

$$\equiv\sum_{\sigma,l,l'}d_{zz\sigma l}^{\dagger}K_{zz}(ll')d_{zz\sigma l'}\,, \quad (4.2a)$$

$$H_0^{xz}=\sum_{l}-\bar{t}(d_{xzl}^{\dagger}P_{zl}+\mathrm{H.c.})\,, \quad (4.2b)$$

$$V^{zz}=\sum_{l}[Un_{zz\uparrow l}n_{zz\downarrow l}-\mu(n_{zz\uparrow}+n_{zz\downarrow})]\,, \quad (4.2c)$$

$$V^{xz}=\sum_{l}[\bar{U}(n_{zz\uparrow l}+n_{zz\downarrow l})n_{xzl}-\epsilon n_{xzl}]\,. \quad (4.2d)$$

In the last equality in Eq. (4.1), an error of order $(\Delta\tau)^2\times$(hopping)$\times$(interaction) has been made, with

hopping $=t,\bar{t}$ and interaction $=U,\bar{U}$. By taking $\Delta\tau$ sufficiently small, this error can be made negligible. In practice, we have taken $\Delta\tau=0.25$ which should give errors of a few (to about 10) percent for the parameter range studied. This was considered sufficient for the purposes of this work.

We have taken the energy of the exciton levels to be $\epsilon_{xz}=-\epsilon$, $\epsilon_{pz}=0$. The results are not very sensitive to the values of these energies as long as the bonding hybridization state lies well below the Fermi level of the d_{zz} band, and the antibonding state well above. We found from our simulations that the best choice for pairing correlations was $\epsilon=\bar{U}\rho$, with $\rho=$band filling.

We eliminate the quartic terms in the exponentials in Eq. (4.1) by introducing auxiliary Ising variables;[23] for the ith time slice,

$$\exp[-\Delta\tau\,\bar{U}(n_{zz\uparrow l}+n_{zz\downarrow l})n_{xz\,l}]$$
$$=\mathrm{Tr}_{\sigma_l^a(i)\sigma_l^b(i)}\{\exp[\bar{\lambda}\sigma_l^a(i)(n_{zz\uparrow l}-n_{xz\,l})+\bar{\lambda}\sigma_{l(i)}^b(n_{zz\uparrow l}-n_{xz\,l})-\tfrac{1}{2}\Delta\tau\,\bar{U}(n_{zz\uparrow l}+n_{zz\downarrow l}+2n_{xz\,l})]\}\ , \tag{4.3}$$

with

$$\bar{\lambda}=2\,\mathrm{arctanh}[\sqrt{\tanh(\Delta\tau\,\bar{U}/4)}]\ , \tag{4.4}$$

and

$$\exp(-\Delta\tau\,Un_{zz\uparrow l})n_{zz\downarrow l}=\mathrm{Tr}_{\sigma_l^c(i)}\{\exp[\lambda\sigma_l^c(i)(n_{zz\uparrow l}-n_{zz\downarrow l})-\tfrac{1}{2}\Delta\tau\,U(n_{zz\uparrow l}+n_{zz\downarrow l})]\}\ , \tag{4.5}$$

$$\lambda=2\,\mathrm{arctanh}[\sqrt{\tanh(\Delta\tau\,U/4)}]\ . \tag{4.6}$$

Equations (4.3)–(4.6) are valid for $U,\bar{U}>0$. We will also study the attractive Hubbard case ($U<0$) for which we use the decoupling

$$\exp(-\Delta\tau\,Un_{zz\uparrow l}n_{zz\downarrow l})=\mathrm{Tr}_{\sigma_l^c(i)}\{\exp[\lambda'\sigma_l^c(i)(n_{zz\,l\uparrow}+n_{zz\,l\uparrow}-1)-\tfrac{1}{2}\Delta\tau\,U(n_{zz\,l\uparrow}+n_{zz\,l\downarrow}-1)]\}\ , \tag{4.7}$$

$$\lambda'=2\,\mathrm{arctanh}[\sqrt{-\tanh(\Delta\tau\,U/4)}]\ . \tag{4.8}$$

Once all the terms in the exponentials are bilinear in fermion operators, we can compute the trace over fermions in the grand-canonical ensemble and obtain an expression for Z which only involves a trace over the Ising variables:

$$Z=\mathrm{Tr}_{\{\sigma_a,\sigma_b,\sigma_c\}}\det[\underline{\mathbb{1}}+\underline{B}_L(1)\underline{B}_{L-1}(1)\cdots\underline{B}_1(1)]\det[\underline{\mathbb{1}}+B_L(-1)B_{L-1}(-1)\cdots B_1(-1)]$$
$$\times\prod_{l=1}^{N}\det(\underline{\mathbb{1}}+\underline{C}_L^l\underline{C}_{L-1}^l\cdots\underline{C}_1^l)\ , \tag{4.9}$$

where $\underline{B}_i(\alpha)$ are $N\times N$ matrices given by

$$\underline{B}_i(\alpha)=e^{-\Delta\tau K_{zz}}e^{\underline{V}_i(\alpha)}\ , \tag{4.10a}$$

$$(e^{V_i(\alpha)})_{ll'}=\delta_{ll'}\exp[\lambda\mu\sigma_l^c(i)+\bar{\lambda}\sigma_l^\alpha(i)-\tfrac{1}{2}(\Delta\tau)(U+\bar{U}-2\mu)]\ , \tag{4.10b}$$

$$\sigma_l^\alpha(m)=\begin{cases}\sigma_l^a(m)\ , & \alpha=+1\\ \sigma_l^b(m)\ , & \alpha=-1\end{cases} \tag{4.10c}$$

and $\underline{C}_i^l$ are 2×2 matrices given by

$$\underline{C}_i^l=\begin{bmatrix}\cosh(\Delta\tau\bar{t}\,)e^{\Delta\tau\epsilon_l'(i)} & \sinh(\Delta\tau\bar{t}\,)\\ \sinh(\Delta\tau\bar{t}\,)e^{\Delta\tau\epsilon_l'(i)} & \cosh(\Delta\tau\bar{t}\,)\end{bmatrix}\ , \tag{4.11}$$

$$\epsilon_l'(i)=\epsilon-\bar{U}-(\bar{\lambda}/\Delta\tau)[\sigma_l^a(i)+\sigma_l^b(i)]\ . \tag{4.12}$$

In addition, we use a checkerboard breakup of the kinetic-energy matrix K_{zz} to speed up the computation,

$$e^{-\Delta\tau K_{zz}}\cong e^{-\Delta\tau K_{zz}^l}e^{-\Delta\tau K_{zz}^2}\ ,$$

where K_{zz}^1 (K_{zz}^2) couples the l odd (l even) sites with the $l+1$ even ($l+1$ odd) sites.

To perform the trace over Ising spins, we need to evaluate the ratio of fermion determinants for configurations that differ by one spin flip, which can be expressed in terms of fermion Green's functions. The calculation is performed efficiently by exactly updating the fermion Green's functions each time a spin is flipped. Details of the algorithm can be found in Ref. 22. It takes $O(N^2)$ operations to update the z-z Green's function, and $O(N)$ operations to update the x-z Green's functions, so that the latter is negligible. For an $N\times L$ lattice, it takes then of the order of $12N^3L$ operations to do one sweep through the lattice. Here the factor 12 = [number of Ising spins per site (3)]$\times$[spin multiplicity of zz electrons (2)]$\times$[number of operations to update each element of zz Green's function (2)].

We have computed the correlation functions defined in Eq. (2.2). Consider for example the average of the product of two density operators:

$$\langle n_{l\sigma}(\tau)n_{j\sigma'}(0)\rangle=\langle\langle d_{l\sigma}^\dagger(\tau)d_{l\sigma}(\tau)d_{j,\sigma}^\dagger(0)d_{j\sigma'}(0)\rangle_f\rangle_c\ . \tag{4.13}$$

In the above equation, $\langle\ \rangle_f$ indicates trace over fermions for a fixed Ising spin configuration, with Boltzmann weight given by the product of the exponential

factors discussed above. The outer $\langle\ \rangle_c$ indicates the sum over Ising spin configurations, with weight given by the product of fermion determinants. Because the Boltzmann weight in $\langle\ \rangle_f$ is a product of exponentials of *bilinear* forms in fermion operators, it is easy to show that Wick's theorem applies, and one obtains

$$\langle d^\dagger_{l\sigma}(\tau)d_{l\sigma}(\tau)d^\dagger_{j\sigma'}(0)d_{j\sigma'}(0)\rangle_f = \langle d^\dagger_{l\sigma}(\tau)d_{l\sigma}(\tau)\rangle_f\langle d^\dagger_{j\sigma'}(0)d_{j\sigma'}(0)\rangle_f + \langle d^\dagger_{l\sigma}(\tau)d_{j\sigma'}(0)\rangle_f\langle d_{l\sigma}(\tau)d^\dagger_{j\sigma'}(0)\rangle_f \ . \quad (4.14)$$

Note that Wick's theorem applies only *inside* the spin configuration average $\langle\ \rangle_c$, where we have free fermions interacting with a fixed external field configuration. Doing the configurational average $\langle\ \rangle_c$ restores the original interactions between the fermions, and Wick's theorem of course fails to apply to the left side of Eq. (4.13).

For our problem, the second term in Eq. (4.14) is nonzero only for $\sigma=\sigma'$. It is easy to show that

$$\langle d_{l\sigma}(\tau)d^\dagger_{j\sigma}(0)\rangle = (\underline{B}_m(\sigma)\underline{B}_{m-1}(\sigma)\cdots\underline{B}_1(\sigma) \times[\underline{\mathbb{1}}+B_L(\sigma)\cdots B_1(\sigma)]^{-1})_{lj} \ , \quad (4.15a)$$

and

$$\langle d^\dagger_{l\sigma}(\tau)d_{j\sigma}(0)\rangle = ([\underline{\mathbb{1}}+\underline{B}_L(\sigma)\cdots\underline{B}_1(\sigma)]^{-1} \times\underline{B}_L(\sigma)\underline{B}_{L-1}(\sigma)\cdots\underline{B}_{m+1}(\sigma))_{jl} \ , \quad (4.15b)$$

where $m=\tau/\Delta\tau$. For computing the susceptibilities then we average products of the matrix elements given in Eqs. (4.15) over the configurations generated in the Monte Carlo sweeps. For the noninteracting case, our procedure is exact for equal time correlation functions, but for the susceptibilities a small error is made in discretizing the time integral in Eq. (2.2). Performing the time integral using Simpson's rule, we found this error to be negligible for $\Delta\tau\leq 0.25$. We have compared our numerical results with exact results for chains of up to 20 sites for the noninteracting case, and with exact results for a two-site system for the interacting case as a check on our simulation program. The agreement was always within a few percent for all quantities with $\Delta\tau=0.25$ and interaction parameters ~ 2, and was improved by taking smaller $\Delta\tau$, thus indicating that the program was running properly. We have studied lattices of up to 24 spatial sites and temperatures down to $\beta=6$. A typical run involved 200 warm-up sweeps and 1000 measurement sweeps.

Figure 15 shows the behavior of CDW and SP susceptibilities as the temperature is lowered in a 20-site lattice. The parameters here were $\overline{U}=2.83$, $\overline{t}\tau=2$, $\epsilon=\overline{U}/2$, $\rho=0.5$ (throughout this paper we measure energies in units of $t=1$). Note that this set of parameters implies $\overline{U}^2/4\overline{t}=1$. The CDW susceptibility is enhanced with respect to the noninteracting case, and shows a peak at $2p_F$ increasing as the temperature decreases (Peierls instability). The exciton interaction also enhances the $q=0$ pairing susceptibility, as shown in Fig. 15(b). Actually, the case shown in Fig. 15 is in principle unfavorable for CDW correlations since $\overline{t}$ is fairly large and the band is not half full. However, as we see from these figures it is difficult to obtain enhanced pairing correlations without simultaneously enhancing $\chi_{\rm CDW}(2p_F)$.

As discussed in Sec. II, the relevant question to ask is which susceptibility diverges faster as the temperature is lowered. Similarly as discussed in Sec. II for the noninteracting case, we study the susceptibilities on lattices of increasing size with β increasing proportionally so that the ratio of temperature to level spacing remains approximately constant. Figure 16(a) shows a case that is particularly favorable for CDW correlations. Here, $\rho=1$, $\overline{t}=0.5$, $\overline{U}=2.82$, and $\epsilon=\overline{U}$. It can be seen that SP is almost negligible on the scale of CDW. In fact, CDW rises very rapidly because the system is developing long-range order. Figure 16(b) shows the static staggered charge-density-wave correlation function at low temperatures, which clearly displays the long-range order. This is similar to what occurs in a related model with phonon instead of exciton degrees of freedom.[27] In addition, examination of typical configurations of the Ising spins clearly shows staggered order developing at low temperatures. This result, obtained from our simulation, is in full agreement with the theoretical expectations discussed in Sec. III.

From the theoretical discussions of the previous sections, it is clear that the first thing to do to suppress the strong CDW correlations is to move away from the $\frac{1}{2}$-filled case, where umklapp is dominant. We also need a

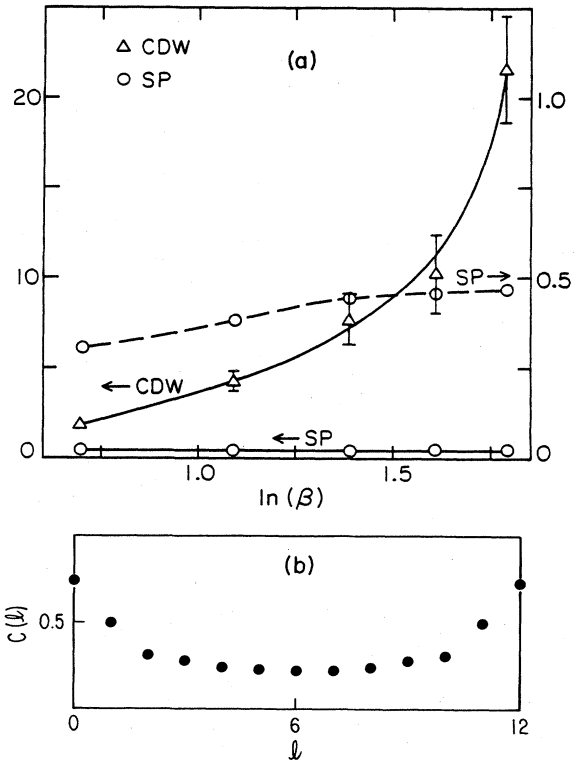

FIG. 16. $\overline{U}=2.83$, $\overline{t}=0.5$, $\epsilon=\overline{U}$, $U=0$, and $\rho=1$. (a) $\chi_{\rm SP}(0)$ and $\chi_{\rm CDW}(2p_F)$ versus $\ln\beta$. Lattice sizes are $N=8$, 12, 16, 20, 24, and $\beta=N/4$. The dashed line shows $\chi_{\rm SP}(0)$ on the enlarged right-hand scale. (b) Static staggered CDW correlation function $C(l)=(1/N)\sum_i(-1)^l\langle n_{zzi}n_{zz,i+l}\rangle$ for $N=12$ and $\beta=6$.

larger $\bar{t}$ since as we have seen a small $\bar{t}$ suppresses SP correlations and does not affect CDW correlations. However, an overly large $\bar{t}$ is not useful since the effective interaction decreases with $\bar{t}$ [Eq. (3.13)]. Figure 17 shows the susceptibilities in a case that should be more favorable to SP correlations: $\rho=0.5$, $\bar{U}=2.83$, $\bar{t}=2$, and $\epsilon=\bar{U}/2$. Indeed, in the nonretarded limit described by an attractive Hubbard model with $U_{\text{eff}}=-\bar{U}^2/4\bar{t}=-1$, $\chi_{\text{SP}}(0)$ would diverge more rapidly than $\chi_{\text{CDW}}(2p_F)$. However, as we will see, we are not yet in the nonretarded limit and as shown in Fig. 17, $\chi_{\text{CDW}}(2p_F)$ and $\chi_{\text{SP}}(0)$ have a rather similar behavior.

To understand what is happening, we consider the behavior of the susceptibilities as a function of $\bar{t}$, for fixed $\bar{U}=2.83$, in the $\frac{1}{4}$-filled case. The solid curve in Fig. 18(a) shows the SP susceptibility for the exciton model on a 20-site lattice with $\beta=5$. The dashed line is the result that would be obtained if the interaction was instantaneous instead of retarded. It was obtained by simulating an attractive Hubbard model with $U_{\text{eff}}=-\bar{U}^2/4t$. Note how $\chi_{\text{SP}}(0)$ for the attractive Hubbard model increases as $\bar{t}$ is decreased and $(-U_{\text{eff}})$ increases. However, the SP susceptibility for the exciton model increases only slightly as $\bar{t}$ is lowered for large $\bar{t}$ and is rapidly suppressed for small $\bar{t}$, as retardation becomes important. For $t\gtrsim 3$, the results of both calculations coincide, indicating that retardation has become unimportant. Figure 18(a) clearly illustrates the problem we are facing. Unless $\bar{t}$ is comparable to the bandwidth, retardation strongly suppresses SP correlations. In contrast, Fig. 18(b) shows the effect of $\bar{t}$ on the CDW susceptibility. The results for the instantaneous case are essentially the same as for the retarded case, and CDW correlations increase rapidly as $\bar{t}$ is lowered because the effective interaction increases.

It is interesting to contrast the scale on which retardation suppresses $\chi_{\text{SP}}(0)$ and the variation of T_c with the characteristic frequency of the pairing interaction as obtained in the usual strong-coupling retarded theory of superconductivity. Assuming a pairing interaction of the form given by Eq. (3.4) we have computed T_c as a function of $2\bar{t}$ for $\bar{U}^2=8$ using the Owen-Scalapino[28] formulation of the Eliashberg[29] equations. The results for T_c versus $\bar{t}$ are shown in Fig. 19. As is well known, the peak in T_c occurs for a value of $\bar{t}$ which is small compared with the bandwidth. In the present case, Fig. 19 shows that T_c peaks for $\bar{t}/t\cong 0.25$. However, our numerical simulation, Fig. 18(a), show that even for frequencies $\bar{t}$ a factor of 4 larger than this, the effects of retardation lead to a suppression of the $\chi_{\text{SP}}(0)$ response. The reason is of course that in 1D there is a competing $\chi_{\text{CDW}}(2p_F)$ instability which, as discussed in Sec. III is enhanced by retardation while the pairing is suppressed. Thus a small amount of retardation can tip the delicate balance to a state favoring CDW. To obtain a clear dominance of SP over CDW correlations in the exciton model, we need to go to a regime where $\bar{t}\gtrsim$ bandwidth $4t$ and the effective interaction is not overly weak. However this requires $\bar{U}\gg$ bandwidth and it becomes difficult to obtain accurate low temperature results from simulations with such large parameters. Instead, we will examine the attractive Hubbard model, which is equivalent to the exciton model

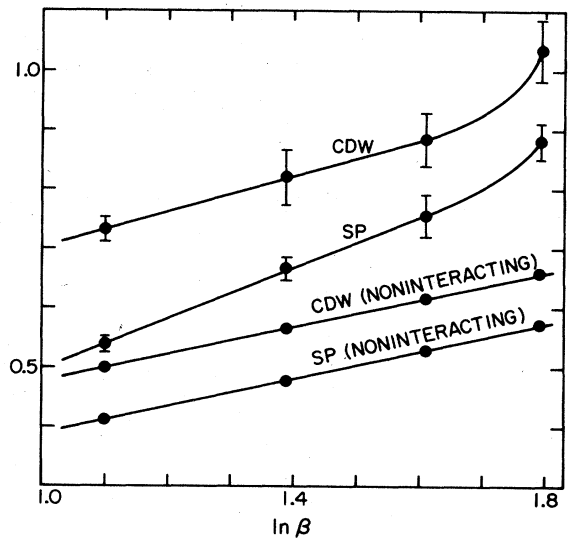

FIG. 17. $\bar{U}=2.83$, $\bar{t}=2$, $\epsilon=\bar{U}/2$, $U=0$, and $\rho=0.5$. $\chi_{\text{SP}}(0)$ and $\chi_{\text{CDW}}(2p_F)$ versus $\ln\beta$. $N=12$, 16, 20, 24, and $\beta=N/4$.

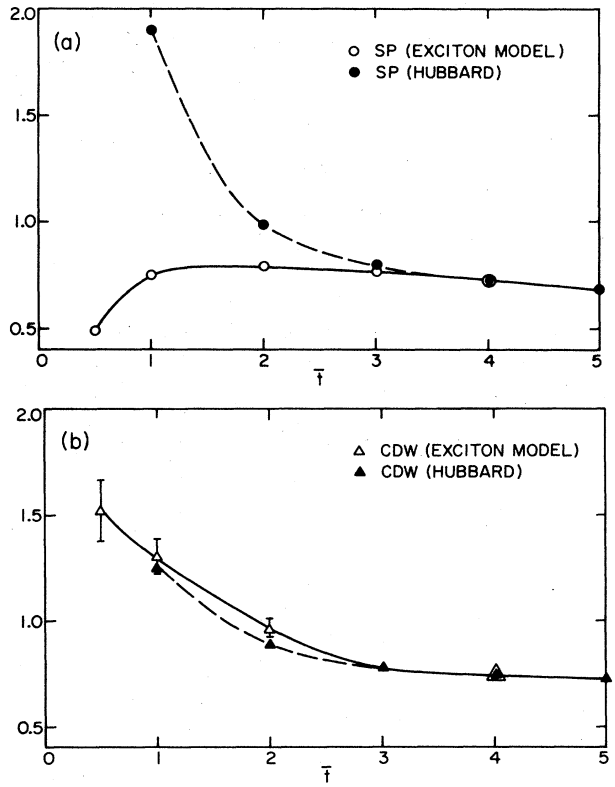

FIG. 18. Susceptibilities versus $\bar{t}$ on a 20-site lattice, $\beta=5$. $\bar{U}=2.83$, $\epsilon=\bar{U}/2$, $U=0$, and $\rho=0.5$. (a) $\chi_{\text{SP}}(0)$ for the exciton model (solid line) and for an attractive Hubbard model with $U_{\text{eff}}=-\bar{U}^2/4\bar{t}$ (dashed line). The difference between both curves shows the effect of retardation. (b) $\chi_{\text{CDW}}(2p_F)$ for the exciton model (solid line) and the attractive Hubbard model (dashed line). Note that retardation has essentially no effect on the CDW susceptibility.

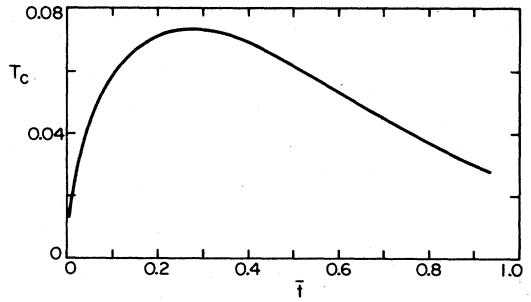

FIG. 19. T_c versus $\bar{t}$ calculated using the Eliashberg equations with an effective interaction given by Eq. (3.4) with $\bar{U}^2=8$.

for large $\bar{t}$, as we showed in Fig. 18.

Figure 20 shows the susceptibilities for an attractive Hubbard model with $U_{\rm eff}=-2$. Here, SP clearly dominates over CDW. In addition, the power-law divergence of the susceptibilities is rather accurately given by the predictions of the renormalization group for this case: $\mu_{\rm SP}=1.2$, $\mu_{\rm CDW}=0.74$.

So far we have neglected the effect of the repulsive Coulomb interaction U between the d_{zz} electrons. However, as emphasized in the discussion, the coupling U is related to $\bar{U}$ by Clebsch-Gordan coefficients, and hence it is unphysical to keep $\bar{U}$ while setting $U=0$. Figures 21(a)–21(d) show the susceptibilities as functions of U for $\bar{U}=2.82$, $\bar{t}=2$, $\rho=0.5$. Note how U rapidly suppresses both SP and CDW correlations, while it enhances SDW correlations. We have also studied a singlet-pairing extended (SPX) correlation function defined by

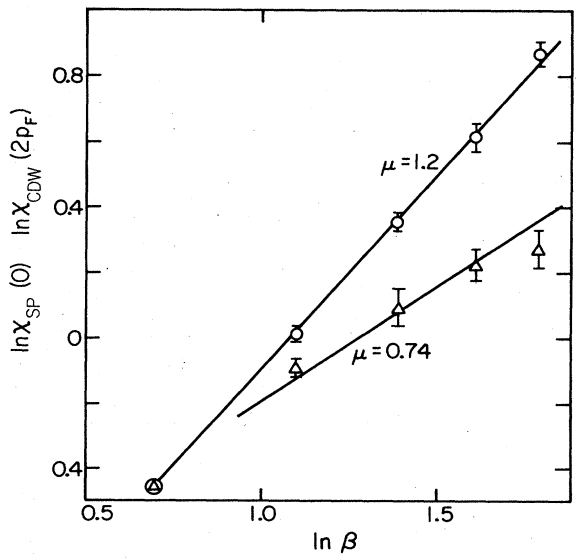

FIG. 20. Susceptibilities for an attractive Hubbard model, $U_{\rm eff}=-2$, $\rho=0.5$, versus β in a log-log plot. $N=8$, 12, 16, 20, 24, $\beta=N/4$. $\chi_{\rm SP}(0)$ diverges more rapidly (slope$=\mu=1.2$) than $\chi_{\rm CDW}(2p_F)$ ($\mu=0.74$).

$$\mathrm{SPX}(q)=\frac{1}{N}\sum_{l,j}e^{iq(l-j)}\times\int_0^\beta d\tau\langle d_{l\downarrow}^\dagger(\tau)d_{l+1\uparrow}^\dagger(\tau)d_{j\uparrow}(0)d_{j+1\downarrow}(0)\rangle\ , \tag{4.16}$$

since one could expect this correlation function not to be as strongly affected by the on-site Coulomb repulsion as the on-site pairing one. However, our numerical results [Fig. 21(d)] show that this is also strongly suppressed by the local Coulomb repulsion. On the other hand, it is known that an on-site Coulomb repulsion can enhance *bond* charge-density wave instabilities leading to a Peierls distortion of the chain.[30,31]

We have also studied triplet-pairing correlation functions, defined by Eq. (2.2d), which are not suppressed by the Hubbard interaction, as are SP and SPX. Figure 22 shows typical results of the triplet- and singlet-pairing $q=0$ susceptibilities versus U. Here we have plotted the ratio of the susceptibilities in the interacting to the noninteracting case. TP is actually suppressed by the exciton interaction that favors singlet pairing. A repulsive U suppresses the singlet pairing and initially slightly enhances the triplet susceptibilities which are also suppressed for large U. Thus we conclude that the exciton model considered in this paper does not favor triplet pairing.

Finally, we have explored the effect of including coupling between nearest-neighbor d_{xz} and p_z orbitals. We added to the Hamiltonian the term

$$H_{nn}=\bar{V}\sum_l n_{zzl}(n_{xz\,l-1}+n_{xz\,l+1})\ . \tag{4.17}$$

To model a realistic system, we would also add a Coulomb interaction V between neighboring d_{zz} orbitals. However, we have not done this, since we wanted to explore what happens as the spatial range of the exciton coupling is increased. Figures 23(a)–23(d) show the effect of a small $\bar{V}$ ($\bar{V}=0.125$) on the SP and CDW correlations. The effect on SP is a slight enhancement with respect to the case $V=0$. However, the effect on CDW is more dramatic, producing a shift of the peak in the susceptibility toward small q. This indicates that the system has a tendency to condense with the compressibility becoming large. As the temperature is lowered however, the peak shifts again toward $2p_F$ indicating that the dominant instability is still Peierls [Fig. 23(d)]. The effect of a larger $\bar{V}$ ($\bar{V}=0.7$) is shown in Fig. 24. Here, up to the lowest temperature studied, the dominant CDW response occurs at $q=0$. The effect on SP correlations is surprisingly much smaller than suggested by the perturbation-theory estimate of Sec. III. Furthermore, although spatially extending the exciton interaction can reduce $\chi_{\rm CDW}(2p_F)$, we find that it produces an undesirable $q=0$ instability in the CDW response. Presumably this would be removed by longer-range direct Coulomb interactions. Clearly modifications such as Eq. (4.18), which extend the range of the exciton mediated interaction, bear further study. However, our initial simulations were not encouraging.

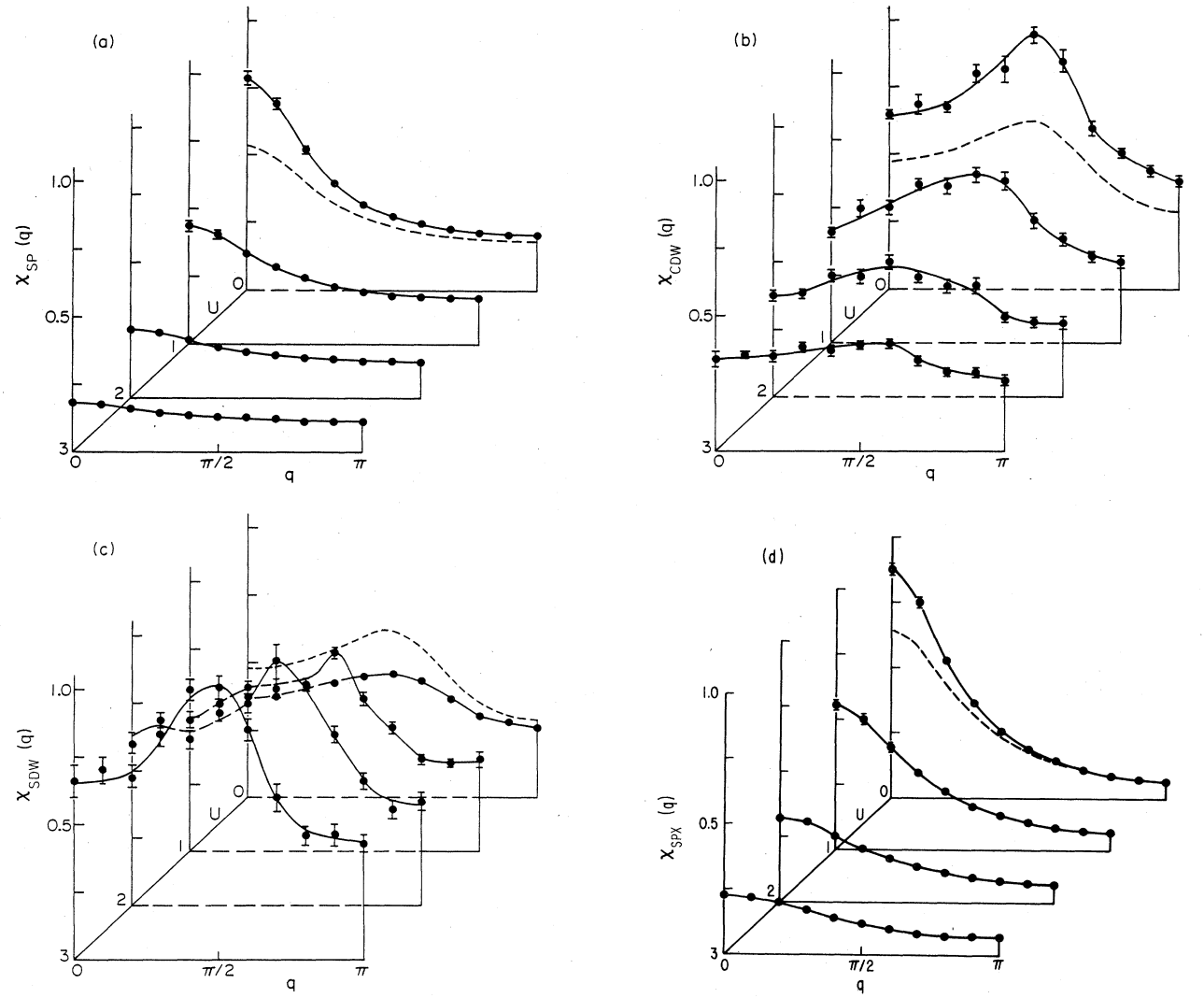

FIG. 21. Susceptibilities versus q for $U=0$, 1, 2, and 3. $\overline{U}=2.83$, $\overline{t}=2$, $\epsilon=\overline{U}/2$, and $\rho=0.5$. (a) $\chi_{SP}(q)$, (b) $\chi_{CDW}(q)$, (c) $\chi_{SDW}(q)$, (d) $\chi_{SPX}(q)$.

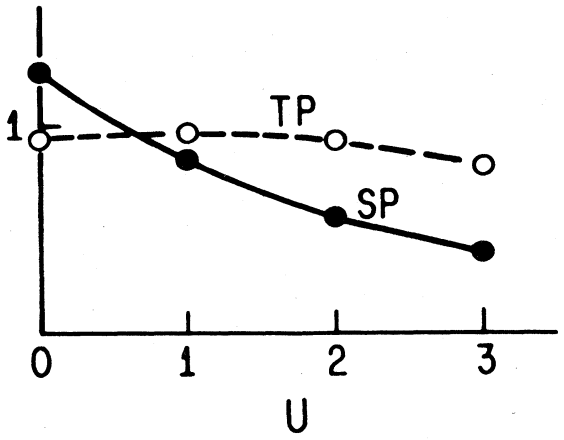

FIG. 22. Ratio of singlet- and triplet-pairing susceptibilities at $q=0$ to their values for the noninteracting case versus U. $\overline{U}=2.83$, $\overline{t}=2$, $\epsilon=\overline{U}/2$, $\rho=0.5$, $N=12$, and $\beta=3$.

V. CONCLUSIONS

We have explored in this paper a model for a quasi-one-dimensional system that we had hoped would show strong enhancement of pairing correlation functions leading to a superconducting instability at temperatures not overly low. The model was introduced by Little as a candidate for an excitonic superconductor and has been extensively discussed over the past 20 years. We have studied the model in various limiting cases (weak-coupling, strong-coupling, and nonretarded limits) using perturbation-theory and renormalization-group results, and for intermediate values of the parameters using a Monte Carlo simulation technique. We thus believe that we understand the properties of the system for all values of the parameters and can make meaningful statements about the likelihood that such a system would display superconductivity. The intermediate-coupling regime, studied by

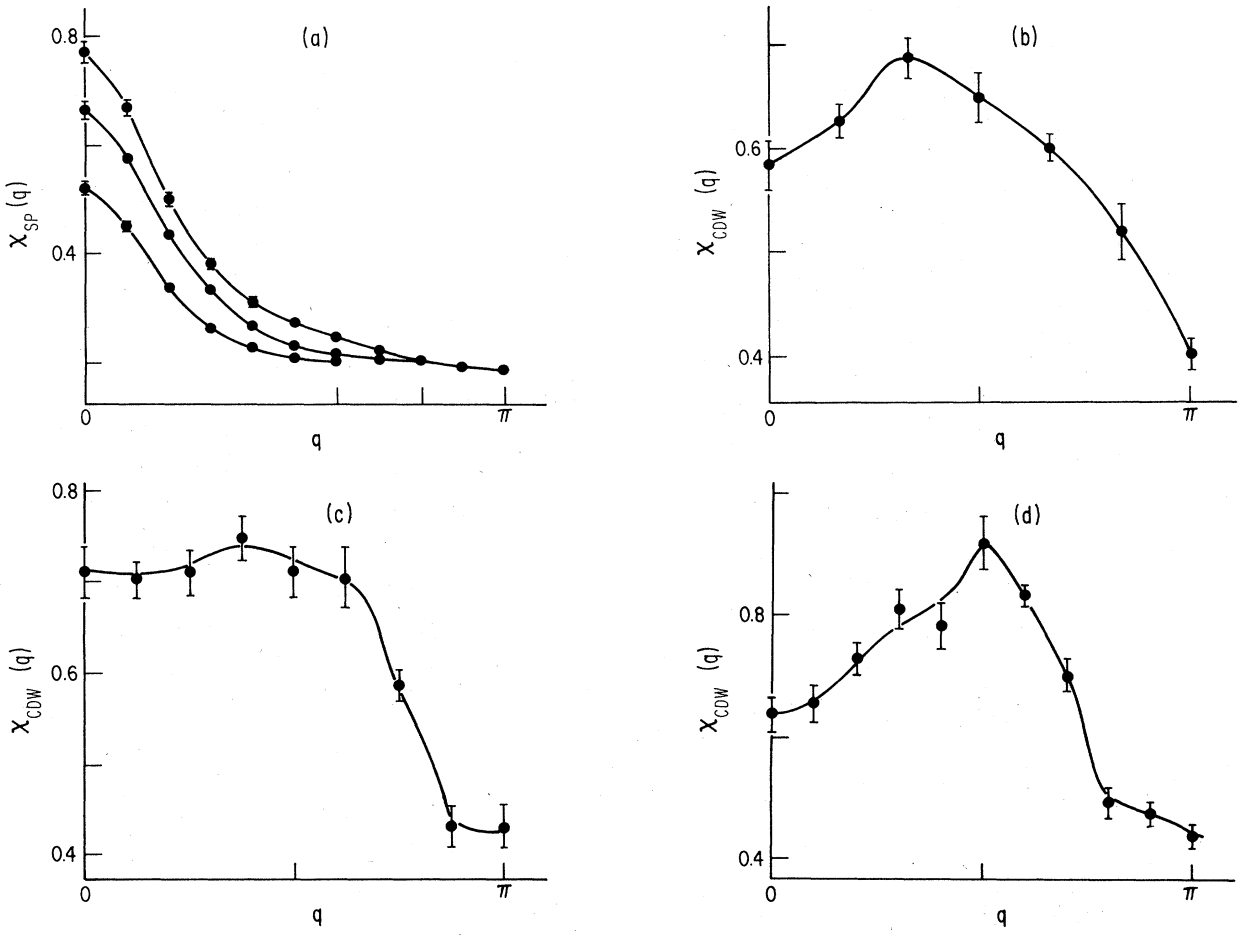

FIG. 23. Effect of nearest-neighbor interaction $\overline{V}$ between d_{zz} and d_{xz} orbitals. $\overline{U}=2.83$, $\overline{t}=2$, $\epsilon=\overline{U}/2$, and $\rho=0.5$. (a) $\chi_{SP}(q)$ versus q for $N=12$ (lower curve), $N=16$, 20, with $\beta=N/4$. (b), (c), and (d): $\chi_{CDW}(q)$ versus q for $N=12$, 16, and 20, respectively; $\beta=N/4$.

Monte Carlo simulations, is probably the most interesting in that it is closest to the parameters that could be attained in a real system.

The first thing to notice is that the model, which consists only of electrons interacting through *repulsive* short-ranged potentials, does show enhancement of singlet-pairing correlations in the Monte Carlo simulations. Of course the model was constructed to have this property, but it still is satisfying to see this confirmed by an exact calculation for finite values of the interaction. However, our results indicate that it is unlikely that such a system would show superconductivity. We summarize our findings in the following.

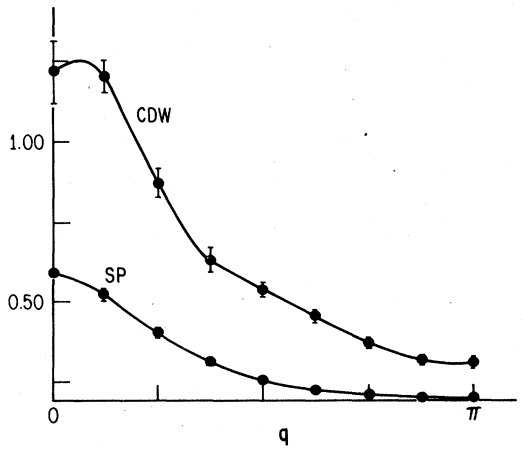

FIG. 24. $\overline{V}=0.7$; other parameters same as in Fig. 25. $\chi_{SP}(q)$ and CDW versus q, $N=16$, $\beta=4$.

(1) For the half-filled-band case and $\overline{t}$ small, CDW clearly dominates and long-range order builds up, both in the conducting spine and on the polarizable ligands. If there is a coupling to lattice degrees of freedom, this would probably be accompanied by a lattice distortion of the same period (dimerization). Pairing correlations decay exponentially in this regime.

(2) For the non-half-filled band, both CDW and SP grow algebraically. However, retardation has a strong effect in suppressing SP correlations while it leaves CDW largely unaffected. Thus, one needs $\overline{t}\sim$ of order the bandwidth or larger to avoid the retardation effects. The usual Eliashberg theory greatly underestimates the effect of retardation in suppressing SP correlations for this model.

(3) The effective interaction is $U_{\rm eff}=-(\bar{U}^2/4\bar{t})+U$ in the nonretarded limit. As discussed above, a small value of $\bar{t}$ does not help to get strong pairing because of the retardation effects. Thus, we need large values of $\bar{U}$. Since U and $\bar{U}$ are proportional in this model, we need $\bar{U}>\bar{t}$, assuming $U=\bar{U}/4$, to get an effective attractive interaction.

(4) However, overly increasing $\bar{U}$ does not help either, as evidenced by our strong-coupling expansion results. For $\bar{U}/\bar{t}\gg 1$, $\bar{t}$ large, the model maps into a highly anisotropic Heisenberg model and the difference $\mu_{\rm SP}-\mu_{\rm CDW}$ becomes small. There seems to be a relatively small optimal range of parameters ($\bar{t}\sim$ bandwidth, $\bar{U}\sim$ a few times $\bar{t}$) that gives the best situation.

(5) Our preliminary simulations of a model which included a nearest-neighbor interaction term between the conducting spine and the side groups did not significantly increase the pairing. In addition, while it did alter the $\chi_{\rm CDW}(2p_F)$ response (when $\bar{V}=0.7$), it led to a large enhancement of the long-wavelength charge-density fluctuations. These, of course, would be suppressed by the long-range Coulomb interactions.

(6) When considering an array of weakly coupled chains of the type discussed here, the possibility for superconductivity appears unlikely. The point is that, as we have seen, for a single chain even when $\chi_{\rm SP}(0)$ dominates over $\chi_{\rm CDW}(2p_F)$, both are expected to diverge as the temperature is lowered. Furthermore, the pairing exponent $\mu_{\rm SP}$ is not so much larger than $\mu_{\rm CDW}$ (see, for example, Figs. 14 and 20). Now, as discussed in Sec. II a direct Coulomb interaction $V_\perp$ can provide an interchain CDW coupling with $V_\perp/t$ of order unity. On the other hand, the pair-transfer coupling will be of order $t_\perp^2/(\bar{U}t)$. As we have seen, in order for a single chain to have $\chi_{\rm SP}(0)$ diverge more rapidly than $\chi_{\rm CDW}(2p_F)$, $\bar{U}$ must be larger than $4t$ so that the pair-transfer coupling is less than $(t_\perp/t)^2$. For the notion of weakly coupled chains to make sense $t_\perp<0.1t$ so that the pair coupling $(t_\perp/t)^2$ is several orders of magnitude smaller than the CDW coupling. Thus even if we are in a regime in which the $\chi_{\rm SP}(0)$ response diverges more rapidly than the $\chi_{\rm CDW}(2p_F)$ response, the 3D CDW transition will occur at a higher temperature unless a mechanism exists to break the CDW coherence between different chains.

In conclusion, we believe our study shows that prospects are not good for building an excitonic superconductor using weakly coupled chains of the type proposed by Little, and explains why such a system has not been found to date despite an extensive search.

ACKNOWLEDGMENTS

This work was supported by the National Science Foundation under Grants Nos. DMR-82-07881 and DMR-83-20481 and by the U.S. Department of Energy under Contract No. DE-AT03-83ER45008. We also gratefully acknowledge E. I. du Pont de Nemours and Company and Xerox Corporation for their support.

APPENDIX: STRONG-COUPLING APPROXIMATION

When the site energies are large compared with the one-electron d_{zz} overlap t, it is sensible to first diagonalize the site Hamiltonian Eq. (3.21) and then use the hopping interaction Eq. (3.24) to lift the site degeneracy. As discussed in Sec. III, in order to have the average d_{zz} filling $\rho=\langle n_{zz\uparrow}+n_{zz\downarrow}\rangle$ different from 0 or 2 requires that μ be given by Eq. (3.23) so that the site ground state is twofold degenerate $E_-(0,0)=E_-(1,1)$. Setting $\epsilon_{pz}-\epsilon_{xz}-\alpha\bar{U}$, the eigenenergies of the site Hamiltonian Eq. (3.22) are

$$
\begin{aligned}
E_-(0,0)&=E_-(1,1)=\frac{\epsilon_{pz}+\epsilon_{xz}}{2}-\left[\left(\frac{\alpha}{2}\right)^2\bar{U}^2+\bar{t}^2\right]^{1/2},\\
E_-(1,0)&=E_-(0,1)=\frac{1}{2}\left[\left(\frac{\alpha\bar{U}}{2}\right)^2+\bar{t}^2\right]^{1/2}+\frac{1}{2}\left[\left(\frac{\alpha-2}{2}\right)^2\bar{U}^2+\bar{t}^2\right]^{1/2}\left[\left(\frac{\alpha-1}{2}\right)^2\bar{U}^2+\bar{t}^2\right]^{1/2}-\frac{U}{2},\\
E_+(1,0)&=E_+(0,1)=E_-(1,0)+2\left[\left(\frac{\alpha-1}{2}\right)^2\bar{U}^2+\bar{t}^2\right]^{1/2},\\
E_+(1,1)&=E_-(1,1)+2\left[\left(\frac{\alpha-2}{2}\right)^2\bar{U}^2+\bar{t}^2\right]^{1/2},\quad E_+(0,0)=E_-(0,0)+2\left[\left(\frac{\alpha}{2}\right)^2\bar{U}^2+\bar{t}^2\right]^{1/2}.
\end{aligned}
\tag{A1}
$$

When $\alpha=1$, the energy-level structure is particularly simple. See Fig. 25, with the excited states separated from the degenerate ground states by gaps

$$
\begin{aligned}
\Delta_-&=E_-(1,0)-E_-(0,0)=\left[\left(\frac{\bar{U}}{2}\right)^2+\bar{t}^2\right]^{1/2}-\bar{t}-\frac{U}{2},\\
\Delta_+&=E_+(1,0)-E_-(0,0)=\left[\left(\frac{\bar{U}}{2}\right)^2+\bar{t}^2\right]^{1/2}-\frac{U}{2},\\
\Delta_2&=E_+(1,1)-E_-(0,0)=2\left[\left(\frac{\bar{U}}{2}\right)^{2/}+\bar{t}^2\right]^{1/2}.
\end{aligned}
\tag{A2}
$$

A strong-coupling expansion begins to be useful when the energy to break a pair $2\Delta_-$ is larger than t. This implies that

$$
2\left[\left(\frac{\bar{U}}{2}\right)^2+\bar{t}^2\right]^{1/2}-2\bar{t}-U>1, \tag{A3}
$$

which reduces to Eq. (3.29). The strong-coupling region in the $(\bar{t},\bar{U})$ plane is shown in Fig. 12 for $U=0$ and $U=\bar{U}/4$.

For an average site occupation $\langle n_{zz\uparrow}+n_{zz\downarrow}\rangle=\rho$, there are $\binom{N}{N\rho/2}$ ways to place the single site ground state pairs.

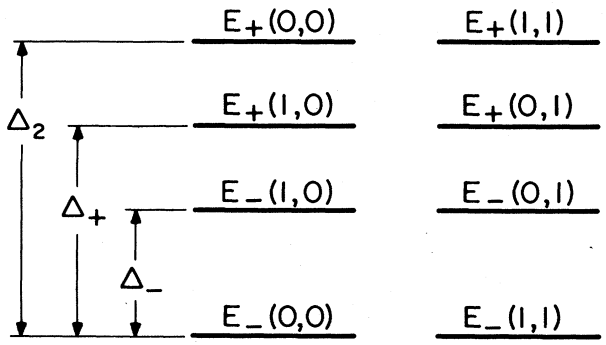

FIG. 25. Energy-level structure of a single site.

This degeneracy is lifted in second order by the hopping interaction,

$$H_t=-t\sum_l (d^\dagger_{zz\sigma l+1}d_{zz\sigma l}+\text{H.c.})\ , \tag{A4}$$

and the strong-coupling problem reduces to diagonalizing the effective Hamiltonian,

$$H_{\text{eff}}=H_t\frac{1}{E_0-H_0}H_t\ , \tag{A5}$$

with $H_0=\sum_l h(l)$ the sum of the site Hamiltonians and $E_0=N\rho E_-(0,0)/2$. H_{eff} can be represented in terms of spin-$\frac{1}{2}$ operators with $n_{zz}=2S_z+1$ so that $S_z=\frac{1}{2}$ corresponds to the doubly occupied ground-state site with energy $E_-(1,1)$ and $S_z=-\frac{1}{2}$ corresponds to the empty ground-state site with energy $E_-(0,0)-E_-(1,1)$. These two degenerate states are coupled via the virtual excitation of the singly occupied site states $E_-(1,0)$, $E_-(0,1)$, $E_+(1,0)$, and $E_+(0,1)$. From the solution of the site Hamiltonian we have the single-site eigenenergies and eigenstates:

$$\begin{aligned}
&E_-(0,0),\quad |\psi_0\rangle=|0,0\rangle_{zz}\otimes|0\rangle \ \text{ with }\ |0\rangle=\frac{|pz\rangle+b\,|xz\rangle}{(1+b^2)^{1/2}}\ ,\\
&E_-(1,1),\quad |\psi_2\rangle=|\uparrow,\downarrow\rangle_{zz}\otimes|2\rangle \ \text{ with }\ |2\rangle=\frac{a\,|pz\rangle+|xz\rangle}{(1+a^2)^{1/2}}\ ,\\
&E_\mp(1,0),\quad |\psi_\mp\rangle=|\uparrow,0\rangle_{zz}\otimes|\mp\rangle \ \text{ with }\ |\mp\rangle=\frac{|pz\rangle+b_\mp\,|xz\rangle}{(1+b_\mp^2)^{1/2}}\ ,
\end{aligned} \tag{A6}$$

with

$$\begin{aligned}
b&=\frac{\alpha\bar U}{2\bar t}+\left[\left(\frac{\alpha\bar U}{2\bar t}\right)^2+1\right]^{1/2},\\
a&=\left(\frac{2-\alpha}{2}\right)\frac{\bar U}{\bar t}+\left[\left(\frac{2-\alpha}{2}\right)^2\left(\frac{\bar U}{\bar t}\right)^2\right]^{1/2}+1\ ,\\
b_\mp&=-\left(\frac{1-\alpha}{2}\right)\frac{\bar U}{\bar t}\pm\left[\left(\frac{1-\alpha}{2}\right)^2\left(\frac{\bar U}{\bar t}\right)^2+1\right]^{1/2}.
\end{aligned} \tag{A7}$$

The effective Hamiltonian, Eq. (A5), can transfer a pair from a full to an empty site via the intermediate states $E_\mp(1,0)$, as illustrated schematically on the left-hand side of Fig. 26. Using the spin-$\frac{1}{2}$ notation, this gives rise to a term,

$$\sum_l\frac{J_x}{2}(S^+_{l+1}S^-_l+S^+_lS^-_{l+1})\ , \tag{A8}$$

with

$$\begin{aligned}
J_x=4t^2\Bigg[&\frac{|\langle-|0\rangle|^2|\langle-1|2\rangle|^2}{2\Delta_-}\\
&+\frac{2\langle0|+\rangle\langle+|2\rangle\langle0|-\rangle\langle-|2\rangle}{\Delta_-+\Delta_+}\\
&+\frac{|\langle+|2\rangle|^2|\langle+|0\rangle|^2}{2\Delta_+}\Bigg].
\end{aligned} \tag{A9}$$

Here the overlap matrix elements are obtained from Eqs. (A6) and (A7). The effective Hamiltonian also contains a $\sum_{l,z}J_zS^x_{l+1}S^z_z$ term which arises from the virtual process shown on the right-hand side of Fig. 26. The energy of a site pair is reduced by the virtual hopping of one electron onto a neighboring site and back. This process can only occur if the neighboring site is empty, otherwise it is blocked by the Pauli principle. A straightforward calculation gives

$$\begin{aligned}
J_z=J_x+\frac{2t^2}{\Delta_-+\Delta_+}\Big(&|\langle+|0\rangle|^2|\langle-|2\rangle|^2\\
&+|\langle-|0\rangle|^2|\langle+|2\rangle|^2\\
&-2\langle2|+\rangle\langle+|0\rangle\\
&\times\langle2|-\rangle\langle-|0\rangle\Big)\ .
\end{aligned} \tag{A10}$$

Plots of J_z/J_x versus $\bar U/\bar t$ for different values of $\epsilon_{pz}-\epsilon_{xz}$

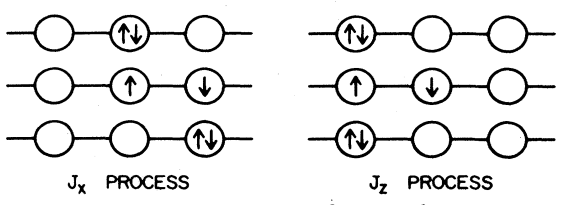

FIG. 26. Schematic illustrations of the configurations which enter in calculating the effective Hamiltonian in the strong-coupling limit.

and U are given in Fig. 13. When $\bar{t}$ is large compared to $\bar{U}$, the splitting between $\Delta_+ - \Delta_- = \bar{t}$ is large and, in addition, the matrix elements in the parentheses of Eq. (A10) tend to cancel so that $J_z \sim J_x$. In this nonretarded limit H_{eff} approaches an isotropic Heisenberg model. However, as shown in Fig. 12, the strong-coupling regime requires $\bar{U} > \bar{t}$ and thus leads to an anisotropic Heisenberg-Ising H_{eff} with $J_z > J_x$.

[1]J. Bardeen, L. N. Cooper, and J. R. Schrieffer, Phys. Rev. **108**, 1175 (1957).

[2]W. A. Little, Phys. Rev. **134**, A1416 (1964); W. A. Little, Int. J. Quantum Chem. **15**, 545 (1981).

[3]H. Gutfreund and W. A. Little, in *Highly Conducting One-Dimensional Solids,* edited by J. T. Devreese, R. P. Evard, and V. E. van Doren (Plenum, New York, 1979), p. 305, and references therein.

[4]Métaux Synthétiques et Organiques, J. Phys. (Paris) Colloq. C3 (1983).

[5]J. J. Solyom, Adv. Phys. **28**, 201 (1979).

[6]V. J. Emery, in *Highly Conducting One-Dimensional Solids,* Ref. 3, p. 305, and references therein.

[7]G. S. Grest, E. Abrahams, S. T. Chui, P. A. Lee, and A. Zawadowski, Phys. Rev. B **14**, 1225 (1976).

[8]J. E. Hirsch and D. J. Scalapino, Phys. Rev. Lett. **53**, 706 (1984).

[9]D. J. Scalapino, Y. Imry, and P. Pincus, Phys. Rev. B **11**, 2042 (1975).

[10]R. A. Klemm and H. Gutfreund, Phys. Rev. B **14**, 1086 (1976).

[11]Similar effects have been discussed within mean-field theory by B. Horowitz, Phys. Rev. B **16**, 3943 (1977).

[12]A. I. Larkin and J. Sak, Phys. Rev. Lett. **39**, 1025 (1977).

[13]L. G. Caron and C. Bourbonnais, Phys. Rev. B **29**, 4230 (1984).

[14]P. Pincus, P. Chaikin, and C. F. Coll III, Solid State Commun. **12**, 1265 (1974).

[15]K. V. Efetov and A. I. Larkin, Zh. Eksp. Teor. Fiz. **69**, 764 (1975) [Sov. Phys.—JETP **42**, 390 (1976)].

[16]V. J. Emery, Phys. Rev. B **14**, 2989 (1976); also see *Highly Conducting One-Dimensional Solids,* Ref. 3.

[17]M. Fowler, Phys. Rev. B **17**, 2989 (1978); *Organic Conductors and Semiconductors,* edited by L. Pal, G. Grüner, A. Janossy, and J. Solyom (Springer, Berlin, 1977), p. 51.

[18]G. Beni, P. Pincus, and J. Kanamori, Phys. Rev. B **10**, 1896 (1974), have discussed a strong-coupling expansion for an electron-phonon system.

[19]A. Alexander and J. Ranninger, Phys. Rev. B **24**, 1164 (1981), discussed bipolaronic superconductivity using related techniques.

[20]J. E. Hirsch and E. Fradkin, Phys. Rev. B **27**, 4302 (1983).

[21]F. D. M. Haldane, Phys. Rev. Lett. **45**, 1358 (1980).

[22]F. Blankenbecler, D. J. Scalapino, and R. L. Sugar, Phys. Rev. D **24**, 2278 (1981); D. J. Scalapino and R. L. Sugar, Phys. Rev. B **24**, 4295 (1981).

[23]J. E. Hirsch, Phys. Rev. B **28**, 4059 (1983).

[24]J. E. Hirsch, Phys. Rev. Lett. **51**, 1900 (1983).

[25]D. J. Scalapino, R. L. Sugar, and W. D. Toussaint, Phys. Rev. B **29**, 5253 (1984).

[26]J. E. Hirsch, D. J. Scalapino, R. L. Sugar, and R. Blankenbecler, Phys. Rev. B **26**, 5033 (1982).

[27]D. J. Scalapino and R. L. Sugar, Phys. Rev. B **24**, 4295 (1981); J. E. Hirsch and E. Fradkin, *ibid.* **27**, 4302 (1983).

[28]C. S. Owen and D. J. Scalapino, Physica **55**, 691 (1971).

[29]G. M. Eliashberg, Zh. Eksp. Teor. Fiz. **38**, 966 (1960) [Sov. Phys.—JETP **11**, 696 (1960)].

[30]J. E. Hirsch, Phys. Rev. Lett. **51**, 296 (1983).

[31]J. E. Hirsch and D. J. Scalapino, Phys. Rev. B **29**, 5554 (1984).